HHS Public Access

Author manuscript

J Magn Reson Imaging. Author manuscript; available in PMC 2018 February 01.

Published in final edited form as:

J Magn Reson Imaging. 2017 February ; 45(2): 337–355. doi:10.1002/jmri.25479.

Diffusion-weighted Breast MRI: Clinical Applications and Emerging Techniques

Savannah C. Partridge, PhD[1,2], **Noam Nissan, MD, PhD**[3], **Habib Rahbar, MD**[1,2], **Averi E. Kitsch, BS**[1,2], and **Eric E. Sigmund, PhD**[4]

[1]Department of Radiology, University of Washington School of Medicine, Seattle, WA 98195, USA

[2]Breast Imaging, Seattle Cancer Care Alliance, Seattle, WA 98109, USA

[3]Department of Biological Regulation, Weizmann Institute of Science, Rehovot, IL

[4]Bernard and Irene Schwartz Center for Biomedical Imaging, Department of Radiology, New York University School of Medicine, New York, NY 10016, USA

Abstract

Diffusion weighted MRI (DWI) holds potential to improve the detection and biological characterization of breast cancer. DWI is increasingly being incorporated into breast MRI protocols to address some of the shortcomings of routine clinical breast MRI. Potential benefits include improved differentiation of benign and malignant breast lesions, assessment and prediction of therapeutic efficacy, and non-contrast detection of breast cancer. The breast presents a unique imaging environment with significant physiologic and inter-subject variations, as well as specific challenges to achieving reliable high quality diffusion weighted MR images. Technical innovations are helping to overcome many of the image quality issues that have limited widespread use of DWI for breast imaging. Advanced modeling approaches to further characterize tissue perfusion, complexity, and glandular organization may expand knowledge and yield improved diagnostic tools.

Keywords

breast diffusion-weighted MRI; breast cancer diagnostics; breast physiology; breast DWI artifacts; diffusion tensor imaging; intravoxel incoherent motion

INTRODUCTION

Breast MRI is a highly sensitive imaging tool for breast cancer detection, and has gained clinical acceptance for a range of clinical indications, including supplemental screening for women at high risk of developing breast cancer and pre-operative evaluation of extent of newly diagnosed breast cancer. However, standard contrast-enhanced breast MRI utilized in

Address Correspondence and Reprint Requests To: Savannah Partridge, PhD, Research Professor of Radiology, University of Washington School of Medicine, Seattle Cancer Care Alliance, 825 Eastlake Ave. E., G3-200, Seattle, WA, 98109-1023, Phone: (206) 288-1306, Fax: (206) 288-6556, scp3@u.washington.edu.

general clinical practice provides only modest specificity, therefore exposing many patients to unnecessary biopsies and limiting its clinical use and acceptance across institutions.

Over the past decade, there has been increasing interest in the use of diffusion-weighted imaging (DWI) for oncology applications. DWI is an advanced MRI technique that can measure the mobility of water molecules diffusing in tissue, which is impacted by biophysical characteristics such as cell density, membrane integrity, and microstructure. Technical advantages of DWI include a short acquisition time (typically 2–3 minutes), wide availability on most commercial scanners, and no need for administration of any contrast agent. Given these advantages and the ability to measure distinct and possibly complementary biological properties to conventional dynamic contrast enhanced (DCE) MRI, DWI increasingly has been studied for breast imaging applications. Promising data from multiple single center studies demonstrate value of DWI for the detection and characterization of breast cancer (1).

BREAST DWI BASICS

DWI is performed using motion-sensitizing gradients to measure the Brownian motion (or random movement) of water molecules. *In vivo*, the diffusion path of water molecules is impeded by the presence of cellular membranes and other obstacles, and thus is not truly random. In this way, water diffusivity in tissue is inversely correlated with the tissue cellularity and the integrity of cell membranes. It is typically performed using a spin-echo prepared sequence with an additional pair of diffusion gradient pulses on either side of the 180° refocusing pulse, Figure 1, based on methods originally proposed by Stejskal and Tanner (2). Diffusion gradients are typically applied in at least three orthogonal directions to obtain rotationally invariant measures. Multiple factors determine the sensitivity of the diffusion sequence to water motion, the primary of which is the degree of diffusion weighting, described by the b-value (unit s/mm^2), given by:

$$b=\gamma^2 G^2 \delta^2 (\Delta - \delta/3) \quad (1)$$

where γ is the proton gyromagnetic ratio, G is the gradient strength, δ is the gradient duration, and Δ is the time delay between the leading edges of the two diffusion-sensitizing gradients (Figure 1) (3). Water protons that change location between the timing of the gradients will not be properly phased at the time of readout. As a result, the MR signal is reduced in intensity proportionally to the water mobility, and for free molecular diffusion this signal decay can be described by the monoexponential equation:

$$S(b)=S_0 e^{-b*ADC} \quad (2)$$

Where S(b) is the signal intensity with diffusion weighting b, S_0 is the signal intensity without diffusion weighting, and ADC is the apparent diffusion coefficient (mm^2/s) (3). *In vivo*, the diffusion process is not free and is modulated by a combination of mechanisms (diffusion, microstructural hindrances, microcirculation) that all contribute to the degree of

signal attenuation. Nonetheless, in vivo signal decay remains relatively monoexponential within intermediate b value ranges with only a modified diffusivity, leading to the term 'apparent' diffusion coefficient (ADC). In general, determination of ADC is performed by acquiring images at multiple b values and fitting the corresponding signal intensities to Equation 2. In the simplest approach, ADC can be calculated directly (without fitting) from only two b values, using:

$$\mathrm{ADC}=\ln(S_1/S_2)/(b_2-b_1) \quad (3)$$

where $b_1 < b_2$ (e.g., $b_1 = 0$ s/mm^2, $b_2 = 1000$ s/mm^2), S_1 and S_2 are the signal intensities at $b = b_1$ and b_2, respectively (4). ADC is calculated for each voxel in the image and presented as a parametric map, Figure 2.

Numerous DWI studies have shown that malignant breast lesions typically exhibit decreased water diffusion, appearing brighter on diffusion-weighted images and darker on ADC maps compared to normal fibroglandular tissue (Figure 2). This reduced diffusion is attributed primarily to increased cell density, resulting in increased hindrance of water motion in the tortuous extracellular space and increased volume of restricted intracellular fluid (5, 6). By comparison, adipose tissue exhibits very low diffusion rates, nearly 10 fold lower than breast fibroglandular tissue, due to restricted water mobility (7), while simple cysts exhibit higher diffusion rates due to the relatively unrestricted microenvironment (5).

STANDARD DWI ACQUISITION AND CHALLENGES

Most DWI sequences utilize an echo planar imaging (EPI)-based readout. The EPI technique is used to achieve very fast image acquisition in order to minimize effects of subject motion and retain high signal-to-noise ratio (SNR). However, EPI is prone to artifacts such as ghosting, chemical shift, and distortions, particularly at higher field strengths (8). These issues are further magnified for breast DWI due to the particular challenges of off-isocenter imaging, air-tissue interfaces, and significant fat content in the breast.

With conventional single shot EPI, all k-space lines that form an image are acquired during a single excitation using an alternating gradient echo readout trajectory. As a result, alternate lines of k-space data must be reversed prior to Fourier transformation, which can introduce phase mismatch from a number of sources including deviation in the linear gradient course, eddy currents, or inadequate shimming. Phase mismatch can manifest as a Nyquist ghost artifact, appearing as a reduced intensity image that is shifted in the phase direction by half the FOV. Inadequate fat suppression is a common problem in breast DWI, often related to poor shimming, and with EPI this results in detrimental chemical shift artifact that can overlay the area of interest. Furthermore, fat suppression techniques cannot eliminate all fat signal, which can contaminate breast tissue ADC measures on a subvoxel level (9, 10). This residual fat signal may need to be considered within advanced modeling and quantitative applications. Magnetic susceptibility differences and other sources of static field inhomogeneities cause nonlinear spatial distortions in the images due to phase error accumulation during the long EPI readout echo train. Such distortions hinder direct

comparison of the DWI data with anatomical images and other functional imaging maps, such as DCE MRI. Several common breast DWI artifacts are illustrated in Figure 3. Eddy-currents induced during application of the strong diffusion gradients cause additional image distortions in the direction of the applied gradients, resulting in misregistration between the different diffusion-weighted images at each slice level and inaccuracies in ADC calculation (8), Figure 4.

Advanced radiofrequency coil design, parallel imaging, and improved shimming techniques during acquisition can help to overcome multiple image quality challenges. Parallel imaging techniques to shorten echo train lengths have been shown to minimize susceptibility-related EPI artifacts in DWI and improve image quality, particularly at 3T (11, 12). Alternate acquisition strategies can further improve image quality for breast DWI. For example, a twice-refocused diffusion preparation has been utilized as an alternative to the standard Stejskal–Tanner spin echo technique to reduce eddy current effects in breast DWI (13). Other technical innovations to achieve high-quality breast DWI are described in Emerging Techniques below.

Post-processing solutions may also improve image quality of conventional DWI for breast imaging. Field mapping approaches utilize an additional MR acquisition to calculate magnetic field or voxel displacement maps, which can be applied to correct susceptibility-related EPI distortions. One correction method utilizes the symmetry of the distortions arising from opposite phase encoding polarities (e.g., anterior-posterior vs. posterior-anterior) to determine the distortion field that unwarps the DWI images. This practical approach requires acquisition of an additional non-diffusion weighted image volume ($b = 0$ s/mm^2) with reversed phase encoding polarity, which takes only seconds of additional scan time, and has recently shown potential for distortion correction in breast DWI (14). Image registration techniques are also useful to reduce spatial misalignment between individual diffusion weighted images due to patient motion or eddy-current–based distortions (8). Such techniques have been shown to improve accuracy for breast DWI (15, 16). However, up to 10% of breast DWI scans in one study exhibited detrimental spatial mismatch between the DW images that could not be corrected by a registration algorithm (17), emphasizing the importance of implementing techniques to minimize patient motion and eddy-current effects at the time of acquisition.

CLINICAL APPLICATIONS

Lesion Diagnosis and Characterization

To date, the greatest evidence and most widely explored application of DWI for breast imaging is as an adjunct sequence to reduce false positives on conventional contrast-enhanced breast MRI. Numerous groups have demonstrated significantly lower ADC values in malignant versus benign lesions. A meta-analysis of 13 individual studies on DWI diagnostic performance demonstrated pooled sensitivity of 84% (95% confidence interval [CI]: 82%, 87%) and specificity of 79% (95% CI: 75%, 82%) in discriminating malignant from benign lesions (total of 964 breast lesions, 615 malignant and 349 benign) (18). DWI images for a variety of MRI-detected breast lesions are shown in Figure 5. Another meta-analysis of 14 studies confirmed that ADC measures are complementary to DCE MRI

parameters for classifying suspicious breast lesions and can increase the accuracy of conventional breast MRI assessment (19). More recently, Bickelhaupt et al reported that DWI may also be useful as a fast and noninvasive approach to assess the likelihood of malignancy for suspicious lesions detected on screening x-ray mammograms and reduce unnecessary biopsies (20). Variations in DWI approach across studies have prevented determination of a generalizable ADC threshold value for the classification of malignant and benign lesions, in particular due to dependence of lesion ADC measures on choice and combination of b values (21). Compiling data from 26 breast DWI studies, Dorrius et al. (22) recently showed that sensitivity and specificity are not significantly affected by choice of b value, but suggested a maximum b value of 1000 s/mm^2 may be optimal for distinguishing benign and malignant lesions. Their analysis further confirmed that contrast agent administration does not significantly affect breast lesion ADC values for the wide range of imaging strategies included.

As the field of oncology pursues personalized and targeted approaches to therapies, accurate tumor characterization, both in terms of histologic composition and biological aggressiveness, is essential for selecting appropriate treatment. DWI reflects tissue microstructure, and emerging evidence suggests that quantitative ADC assessment may help to differentiate tumor subtypes. One would expect that lower ADCs in general would correlate with more aggressive invasive breast cancer phenotypes (with higher proliferation and cellularity). Indeed, a large study evaluating 290 invasive breast cancers by Choi et al. found lower ADC to be significantly associated with higher proliferation (based on the Ki-67 index) (23), which has been reiterated in a number of subsequent studies (24–26). Jiang et.al. recently found strong negative correlation between cellularity and ADC values in a cohort of 29 benign and 59 malignant breast lesions (27). A negative association has also been demonstrated between ADC and tumor grade in several studies (28–30). Interestingly, although estrogen receptor (ER)-positive breast cancers are in general associated with a better prognosis than ER-negative cancers, several authors have found ER-positivity to be associated with lower ADC values (23, 31–35). However, correlations of ADC with prognostic factors have been inconsistent to date, with many studies finding no significant associations.

Studies examining DWI features for biological characterization of DCIS have yielded similarly promising results. Identification of valuable DWI markers of DCIS biology is clinically important, as it would help to reduce overtreatment of this pre-invasive disease. On DWI, DCIS typically exhibits higher ADC values than invasive cancer (23, 36), presumably owing to lower cellularity. Multiple studies have reported DCIS lesions diagnosed on core needle biopsy that upgrade to invasive disease on surgical excision demonstrate lower ADC values than those that do not upgrade (37–39). Among pure DCIS lesions, several individual studies have shown DWI characteristics to differ between high and low nuclear grade (36, 40, 41), although the reported performance of ADC to distinguish among these subtypes has been variable. Overall, studies with larger cohorts from multiple institutions are needed to better determine the potential role of DWI as a reliable breast cancer biomarker that can guide therapies.

Axillary Lymph Nodes

Surgical staging of the axilla is highly accurate but confers significant rates of morbidity, including edema and parasthesia. Thus, there is interest in developing a non-invasive, image-based method to determine the presence or absence of axillary lymph node metastases. While there are no features on DCE MRI that can distinguish malignant from benign nodes with high specificity, several studies have shown promise for the use of DWI to stage the axilla, Figure 6. A recent meta-analysis of 13 studies with 1487 axillary lymph nodes demonstrated overall lower ADC values in metastatic compared to non-metastatic nodes, with sensitivity and specificity of DWI to be 83% and 82%, respectively (42). However, one study evaluating DWI for increasing specificity of conventional breast MRI for diagnosing axillary lymph nodes did not find any differences in ADC between morphologically suspicious malignant and benign reactive nodes (43), and another study reported lymph node diameter measures to be more predictive of involvement than ADC values (44), suggesting more investigation is needed to determine the added value of DWI to standard MR assessment of the axilla.

Monitoring and Predicting Treatment Response

DWI is also being explored for improving the ability to assess therapeutic response. Cytotoxic effects of chemotherapy including cell lysis, apoptosis, and necrosis cause alterations in cell membrane permeability and increase in extracellular space, which lead to a less restrictive environment for water to more freely diffuse. Therefore, it has been hypothesized that an increase in tumor ADC values may reflect favorable treatment response earlier than detectable changes in tumor size, Figure 7. In support of this, several clinical studies have shown early changes in tumor ADC after the first cycle of chemotherapy to significantly differentiate responders from nonresponders (45–47). Galban et al recently demonstrated that parametric response maps of voxel-based changes in ADC may help identify response earlier than whole tumor ADC measures (45). However, while many studies have observed significant increase in breast tumor ADC with treatment, the association with treatment response has been variable. Additionally, pretreatment ADC measures may hold prognostic value to help identify patients who will best respond to neoadjuvant treatments. Three large scale studies of women with locally advanced breast cancer undergoing neoadjuvant chemotherapy (n=519 women total) each showed low pretreatment tumor ADC values to be predictive of pathological complete response for triple-negative tumors, with more variable findings in luminal and HER2+ subtypes (48–50). Overall, there is wide variability in the literature as to the utility of DWI to monitor breast cancer therapy, likely due to differences in study design (including treatment timings of imaging, patient characteristics, and ADC measurement approaches), and further investigation is needed to validate ADC as a predictive biomarker of therapeutic efficacy.

Non-Contrast MR Screening

There may also be a role for DWI as an alternative to contrast-enhanced MRI for breast cancer screening (51–54). Early investigations showed many mammographically and clinically occult breast cancers are visible on DWI and exhibit low ADC values (55), Figure 8. In blinded reader studies, Yabuuchi et al demonstrated that a non-contrast MRI approach

with DWI achieved a higher accuracy for breast cancer detection than mammography (53), and Trimboli et al reported sensitivity of 76% and specificity of 90% for cancer detection on DWI (52). More recently, McDonald et al evaluated the performance of DWI to detect mammographically occult breast cancers specifically in women with dense breasts. This study showed that DWI has the potential to identify as many as 8 additional cancers over mammography per 1000 women screened, with reasonable specificity and positive predictive value (91% and 62%, respectively) (54). Technical optimizations can further improve breast cancer detectability on DWI (56, 57). This screening application is particularly timely given increasing breast density legislation raising awareness of the limitations of mammography in dense breasts (58, 59). Moreover, there are growing health concerns related to the long-term use of gadolinium contrast agents utilized in conventional breast MRI (60). To date, only a handful of studies have explored the utility of DWI for non-contrast screening, but promising preliminary data warrants further investigation.

PHYSIOLOGIC VARIABILITY OF BREAST ADC MEASURES

The breast is an active gland that undergoes a variety of physiologic changes over the course of a woman's lifetime that can affect appearance on imaging. During the menstrual cycle, the breast parenchyma undergoes both vascular and histologic changes (61, 62) in response to hormonal fluctuations. The resulting vascular response can produce enhancement of normal breast parenchyma, termed 'background parenchymal enhancement (BPE),' that may prompt a false-positive finding on DCE MRI (63, 64). Histologically, cyclic differences in luminal and basal myoepithelial cell layers, cellular vacuolization, and interlobular edema have been described (65), which underlie changes in mammographic breast density (66) and screening performance among premenopausal women (67). An early study investigating menstrual cycle effects on breast DWI reported non-statistically significant variations in ADC (intra-subject coefficient of variation = 5.5%) between four weekly measurements in healthy premenopausal volunteers with regular cycles (68). Subsequent studies (69–72) confirmed no significant influence of menstrual phase on ADC values of healthy breast tissue or breast cancers, with one exception (73) finding significant elevation (14%) in luteal phase. Moreover, neither ADC values of normal breast tissue nor breast cancer show correlation with BPE (74–77). Overall, the relative stability of breast ADC measures to cyclic variations suggests DWI may be used at any phase of the menstrual cycle.

During lactation the clinical utility DCE MRI is limited because blood flow is elevated and the normal lactating parenchyma shows increased contrast enhancement (78). Histologically, the lactating breast is characterized by an expanded ductal tree distended with lipid-rich milk (79, 80). Breast tissue ADC values in lactating women are significantly reduced (71), likely due to the high lipid content and viscosity of the milk, but remain higher than that of malignancy (81), suggesting cancer may still be distinguishable on DWI in lactating women despite reduced background diffusivity levels.

Breast density is known to decrease with age, with a gradual atrophy of the fibroglandular tissue occurring after menopause. Several studies have shown breast tissue ADC values to positively correlate with breast density (74, 75). Further, normal breast tissue ADC values in postmenopausal women are generally lower than in premenopausal women (69, 71, 72). The

physiologic basis for this reduction in ADC of normal tissue in older women is unclear, but may be in part related to changes in water content, microcirculation, and adipose content in breast fibroglandular tissue with age. Studies of menopausal effects on lesion ADC values have yielded conflicting results (72, 82).

In summary, physiological modulations such as menopause and lactation can significantly influence ADC values in normal fibroglandular tissue, with less effects observed on tumor ADCs, which should be considered in clinical interpretations. However, the range of normal breast ADC values under all physiological variations appears to remain significantly higher than that of most malignancies and therefore may not compromise diagnostic performance.

EMERGING TECHNIQUES

Alternate Acquisition Strategies

As the clinical utility of DWI for breast evaluation has grown more widespread and well-defined, efforts to maximize its image quality have seen a concomitant rise. While the motion-insensitivity and speed of single-shot EPI currently preserve its role as the most common readout for breast DWI, its artifacts motivate a range of alternatives. Some techniques do not abandon but instead adapt EPI for improved speed, resolution, or quality. Readout-segmented EPI (rs-EPI) alters the conventional EPI trajectory by acquiring all phase encodes but restricting the readout acquisition in each shot as a means of limiting susceptibility artifacts, at the expense of longer scan time and some navigator-corrections. A range of breast DWI studies have employed this approach successfully (83–86), Figure 9. In a related sense, reduced field-of-view (rFOV) approaches aim to reduce the required matrix size, and with it the susceptibility induced signal loss and distortion, for a given resolution by imaging only a subvolume. This approach must either suppress the surrounding regions (outer volume suppression (OVS)) or excite only the target region (inner volume excitation (IVI)). The latter approach (IVI) has found application to breast cancer in a range of studies employing a 2D spectral-spatial excitation (87–90). rFOV is highly applicable for breast lesion assessment where delineation of lesion borders and heterogeneity separate from the surrounding fibroglandular or adipose tissue can be challenging with conventional EPI, Figure 10. Initial studies have shown both quantitative differences (i.e. lower ADC values) and qualitative differences (i.e. better defined border features and regional variations) between rFOV and conventional methods. Finally, simultaneous multi-slice (SMS) approaches use a multiplexed excitation and acquisition approach to dramatically accelerate acquisitions in the slice dimension, and have been used in conjunction with rs-EPI in the breast (85).

Other pulse sequences or k-space trajectories can improve image quality. One single-shot sequence, termed turbo spin echo (TSE), fast spin echo (FSE), or rapid acquisition with relaxation enhancement (RARE), includes a series of spin echoes refocused by RF pulses rather than gradient echoes as in EPI. This approach has the advantage of removing T2*-related signal losses and susceptibility distortions, at the expense of increased T2-weighted signal loss and blurring and additional RF heating. Artifacts can also arise from phases imparted by the diffusion gradients preventing fulfillment of the CPMG condition and causing echo interference (91); these can be solved either by spoiling (92) or separating (93)

echo pathways or modulating RF pulse phases (94). Several studies have employed variants of TSE-DWI for breast evaluation (68, 95–98) and have generally found comparable image quality to EPI with better morphologic agreement with anatomical imaging. However, the drawbacks of TSE-DWI for breast have prevented its widespread replacement of EPI, though technical developments continue.

Another sequence class is steady-state free precession (SSFP), in which a train of pulses maintains a steady-state magnetization with a mixed weighting of relaxation, flip angle excitation, and diffusion. This efficient 3D spin-echo sequence has advantages of image quality and spatial resolution, but also disadvantages of inter-shot phase errors from diffusion gradients that necessitate navigator-correction or other mitigating strategies (99). Also, while the signal contrast is calculable (100), significant supplementary data (T_1, T_2, B_1 maps) are required for ADC quantitation. Pilot studies with dual echo steady-state (DESS) acquisitions have shown interesting morphologic improvements in breast tissues (101), but more development is warranted.

A non-Fourier alternative to EPI is spatio-temporal encoding (SPEN), which involves exciting spins in a spatiotemporally sequential fashion and acquiring signal in the presence of a gradient. Free from Nyquist sampling constraints, SPEN methods utilize dramatically higher acquisition gradients, avoiding many EPI artifacts and providing robustness to field inhomogeneities. Interaction between SPEN's imaging gradients and the diffusion-sensitizing gradients must be taken into account for ADC maps. Recently, SPEN-DWI in the breast showed negligible geometrical distortions, robustness to ghosting artifacts (102) and acceptable specific absorption rate (SAR) levels, demonstrating its potential for expanded use in clinical breast imaging.

High and Ultra-High Field Strengths

Another avenue to improve breast DWI is increasing field strength and capitalizing on the increased magnetization and associated SNR. While 1.5 T scanners may remain the most common platform for breast MRI, 3 T scanners are increasingly prominent and are showing comparable or superior quality for the whole breast exam, including DWI. A comprehensive large-scale comparison of breast DWI between 1.5 T and 3 T has yet to be performed. In the ultra-high field (7 T and above) regime, selected breast DWI studies have been performed with conventional EPI (103, 104) or rs-EPI (105, 106). One rs-EPI study of 28 patients scanned at both field strengths found lower ADC values, higher resolution, equivalent SNR, and comparable diagnostic accuracy at 7 T compared to 3 T (106). Whether the 7 T platform will eventually be used for widespread clinical breast evaluation is yet to be seen, but initial indications are that breast DWI can successfully be performed at 7 T, and the combination of high field strength and sequence innovation can improve its utility.

Advanced DWI Modeling

While the simplicity and ubiquity of the single component isotropic apparent diffusion coefficient (ADC) model, as well as its applicability to cancer diagnosis, have led to its widespread application in breast DWI, there is an increasing use of advanced diffusion techniques to characterize both normal fibroglandular tissue and breast neoplasms. These

approaches include additional sampling and analysis frameworks that capitalize on features such as structural anisotropy (DTI), microvascularity (IVIM), and microstructural complexity (DKI). The use of these methods is motivated by the view that additional specificity in the description of breast tissue will enable more powerful differentiation, classification, and prognostication of disease. Studies exploring these approaches for breast imaging are in early stages, ranging from assessing feasibility to preliminary data collection, and some begin to assess clinical diagnostic power.

DTI: Anisotropy—Water diffusion within biological tissue is often anisotropic due to directionally-dependent restriction imposed by microstructural architecture. Diffusion tensor imaging (DTI) extends standard DWI to characterize the orientational variability of the diffusion process, allowing assessment of diffusion directionality or anisotropy in addition to the diffusion rate (as measured by ADC). DTI requires acquisition of a greater number of diffusion gradient directions, six or more, and expresses the diffusion coefficient as a function of direction in the form of a tensor (107). The calculated DTI tensor parameters include the eigenvalues (λ_1, λ_2, and λ_3), their average (mean diffusivity [MD] or ADC) and associated anisotropy indices expressing variability between the eigenvalues, such as the normalized index of fractional anisotropy (FA).

It has been proposed that the mammary ductal network may impose diffusion anisotropy in healthy fibroglandular tissue, with less restricted water diffusion in directions parallel to the walls of the ducts, which has been investigated by a number of DTI studies (77, 108–111). Malignant transformation may in turn cause blockage of the ducts by proliferating neoplastic cells and loss of structured organization, resulting in a concomitant reduction of anisotropy measures. Indeed, two studies demonstrated FA to be significantly reduced in malignancies versus normal breast tissue (112, 113), Figure 11, although a number of other DTI studies found no difference (114–117). In differentiating breast lesions, a general consensus exists across studies regarding significantly reduced diffusivity (ADC or MD) in malignant tumors versus benign lesions. However, there are conflicting results regarding the diagnostic utility of the anisotropy indices, with several studies reporting lower FA in benign lesions compared to malignant lesions (27, 113, 114, 118) and others finding no difference in FA (112, 115, 116), warranting further investigation. One study (117) reported the eigenvalue difference ($\lambda_1 - \lambda_3$), another measure of anisotropy, to significantly discriminate malignancy. Figure 12 summarizes recent studies reporting DTI metrics in human breast cancers (27, 112–119), with corresponding study characteristics reported in Table 1. The variable findings may be attributable in part to differences across studies in measurement approach, patient cohort, and lesion types characteristics. While the diagnostic value of diffusion anisotropy in breast is still under investigation, the qualitative distinction between structured native fibroglandular tissue and disordered neoplasms has been highlighted by a growing number of breast DTI studies, and continued work may refine characterization of this feature for clinical diagnostics.

Aside from scalar metrics, maps of the primary eigenvector orientation suggest the ability of breast DTI to demonstrate structural organization and illustrate the mammary ductal tree, with primary eigenvector $\hat{e}_1$ generally directed anterior-posteriorly towards the nipple (Fig 11) (71, 111, 114). DTI tractography, which utilizes these eigenvector maps to continuously

trace the three-dimensional trajectories of coherently organized media, was first introduced in the brain to enable visualization of the connectivity of neuronal pathways in vivo (120). Efforts are underway to adapt conventional DTI fiber tracking methods for breast DTI (121), but the feasibility of tractography for delineating the breast ductal network requires further investigation.

IVIM: Microvascularity—The hallmark feature of hypercellularity due to cell proliferation in tumors, and its restriction of water motion, underpins ADC contrast in breast cancer. However, angiogenesis, or the growth of dysfunctional neovasculature supporting that proliferation, is another common feature of aggressive tumors that is not captured in the ADC model and may reduce its contrast when present. The intravoxel incoherent motion (IVIM) model aims to circumvent this conflict by separating contributions from microvasculature and the surrounding parenchyma. One of the oldest in vivo DWI models (122) that is currently in the midst of a dramatic revival for new organs and pathologies (123), the IVIM approach fits a biexponential decay model to the signal b-value dependence. The biexponential analysis allows measurement of the perfusion volume fraction (f_p or f), and separation of the tissue diffusivity (D_t) in the parenchyma from pseudodiffusivity (D_p or D*) in the microvasculature. In the setting of cancer, restricted D_t is a marker of cellularity, f_p of blood volume, and D_p of blood velocity/vessel architecture. The first applications of this approach to breast cancer revealed a measurable vascular contribution in both DCIS and invasive lesions (124), Figure 13, and other studies illustrated much smaller (or negligible) perfusion fractions in fibroglandular tissue (9, 125). This is consistent with the low blood volume of fibroglandular tissue compared to other more vascular organs; thus, the primary application of breast IVIM is in lesion characterization. A range of studies with larger cohorts have begun to highlight the clinical potential of characterizing microvascularity and cellularity separately. Figure 14 shows a summary of 9 studies reporting IVIM metrics in human breast cancers (96, 124–131) recruiting a total of 714 women, with corresponding study characteristics reported in Table 2. Among these studies, 5 showed significantly lower tissue diffusivity D_t in malignant lesions (average sensitivity 86±13%, specificity 81±19%, accuracy 84±12%) (96, 125, 126, 129, 132), and 4 showed significantly higher f_p in malignant lesions (average sensitivity 82±8%, specificity 81±20%, accuracy 84±2%) (96, 125, 126, 132) compared to benign lesions. Some studies (96, 125) indicated advantages of combining parameters for improved diagnostic accuracy. While optimal schemes of acquisition, modeling, and capturing heterogeneity remain under debate, a growing recognition of the IVIM signature in breast lesions and its possible utility is clear.

Non-Gaussian Behavior/DKI: Intravoxel Heterogeneity—Motivated by the complexity of the microenvironment, approaches to capture diffusion behavior beyond a single Gaussian diffusivity have been applied to breast fibroglandular tissue and lesions. For example, preclinical imaging of breast tumor models at high diffusion weighting revealed treatment-sensitive intra- versus extracellular water compartmentalization (133). Clinical radiologic-pathologic correlation has shown inverse correlation between ADC and tumor to stromal ratio (134). The advanced diffusion approaches addressing this complexity can be loosely categorized as employing variable diffusion weighting or variable diffusion time.

Diffusion kurtosis imaging (DKI) quantifies non-Gaussianity ("kurtosis") of the water displacement distribution, which is measurable in a quadratic order expansion of the signal b-value dependence (135). Several recent studies have shown mean diffusional kurtosis to be significantly higher in malignant compared to benign breast lesions (127, 136–138), adding to the diagnostic accuracy of ADC alone, Figure 15. Other approaches posit a distribution of diffusion coefficients leading to a 'stretched-exponential' response (130), which has also delivered diagnostic benefit in excess of diffusion alone. Both approaches typically require sampling higher b-value ranges than DWI, which for normal breast tissue can increase demand for SNR given its high normal diffusivity (~2×10^{-3} mm^2/s). Another important issue of non-Gaussian diffusion quantification is biophysical specificity; unless coupled with an interpretive model (as in neuroimaging (139, 140)), the source of non-Gaussianity can be unclear. Recent *ex vivo* microimaging results in fixed breast tissue showed the range of diffusivities among lobular, ductal, stromal, adipose, and cancerous components that contribute to DWI at conventional resolution (141); such analyses may inform upon the next iteration of advanced breast diffusion imaging.

Diffusion Time Dependence—The other control variable of diffusion contrast is the diffusion time (Δ, Fig 1), which determines the interval of transport allotted to the spins to explore their environment. While for unrestricted Gaussian diffusion the diffusivity is time-independent, barriers in a biological matrix increasingly limit displacement as diffusion time increases. This effect can be exploited for additional contrast and, with a modeling context, microstructural quantification (142). Typical DWI acquisitions have Δ in the range of 35–50 ms, corresponding to an approximate (one dimensional) diffusion displacement $l = \sqrt{2D\Delta}$ of 14–17 μm for unrestricted free water at body temperature (D~3×10^{-3} mm^2/s). Diffusion time was found to affect anisotropy measures of normal fibroglandular tissue, with reduced anisotropy values observed for all indices following shortening of the diffusion time from 47 to 33 ms (117). Another recent DTI study using a stimulated echo approach to achieve diffusion times up to 1 s showed potential for improving the ability to resolve diffusion anisotropy of fibroglandular tissue related to the mammary ducts (143), where ductal lumens can range in scale up to hundreds of μm in diameter. Longer diffusion times may increase differentiation of cancer from normal tissue as well as refine understanding of breast fibroglandular tissue diffusion characteristics. While the emphasis on ductal architecture has been a useful interpretive guide thus far, the variable size and moderate volume fraction of mammary ducts suggests multiple stromal components (collagen, lobules) may also contribute. Indeed, further effort is warranted to disentangle all contributions to breast diffusion anisotropy, with proper attention to signal-to-noise ratio, and employing a wide range of diffusion encoding (strength, direction, diffusion time) may provide a broad supporting database.

CONCLUSIONS

In summary, there is rapidly growing evidence of the potential value of DWI to improve breast cancer detection and characterization. The technique is relatively easy to incorporate into clinical breast MRI protocols and provides complementary information to conventional breast MRI examinations. Furthermore, DWI may have value as an alternate MRI screening

tool for detecting cancer without the need for any contrast agent. Multicenter trials are needed, several of which are currently underway through the American College of Radiology Imaging Network (ACRIN) (144, 145), to validate single-institution findings and to develop generalizable interpretation strategies. With technique standardization and clear interpretation guidelines, the role of DWI for clinical breast imaging is expected to grow in coming years.

Advancements in DWI acquisition strategies are increasingly overcoming the technical issues inherent to standard echo planar imaging, which have heretofore somewhat limited widespread clinical implementation of DWI for breast imaging applications. Moreover, advanced encoding and analysis methods for breast diffusion MRI are helping to broaden understanding of water transport in the breast and may yield better diagnostic tools. While it remains to be seen which contrast mechanisms or workflows may be truly beneficial to current breast imaging practice, tissue features elucidated by tracking water motion remain an aggressively sought target. As innovation continues, we may expect more clinical benefits to emerge for DWI of the breast.

Acknowledgments

Supported by: NIH Grant R01CA151326 (Partridge, PI), and RSNA Research Scholar Grant (Rahbar, PI)

REFERENCES

1. Partridge SC, McDonald ES. Diffusion weighted magnetic resonance imaging of the breast: protocol optimization, interpretation, and clinical applications. Magn Reson Imaging Clin N Am. 2013; 21(3):601–624. PubMed PMID: 23928248; PubMed Central PMCID: PMC3740446. [PubMed: 23928248]
2. Stejskal EOTJ. Spin diffusion measurements:spin echoes in the presence of a time-dependent field gradient. J Chem Phys. 1965; (42):288–292.
3. Le Bihan D, Breton E, Lallemand D, Grenier P, Cabanis E, Laval-Jeantet M. MR imaging of intravoxel incoherent motions: application to diffusion and perfusion in neurologic disorders. Radiology. 1986; 161(2):401–407. Epub 1986/11/01. PubMed PMID: 3763909. [PubMed: 3763909]
4. Le Bihan D, Breton E, Lallemand D, Aubin ML, Vignaud J, Laval-Jeantet M. Separation of diffusion and perfusion in intravoxel incoherent motion MR imaging. Radiology. 1988; 168(2):497–505. PubMed PMID: 3393671. [PubMed: 3393671]
5. Guo Y, Cai YQ, Cai ZL, Gao YG, An NY, Ma L, et al. Differentiation of clinically benign and malignant breast lesions using diffusion-weighted imaging. J Magn Reson Imaging. 2002; 16(2): 172–178. PubMed PMID: 12203765. [PubMed: 12203765]
6. Sinha S, Lucas-Quesada FA, Sinha U, DeBruhl N, Bassett LW. In vivo diffusion-weighted MRI of the breast: potential for lesion characterization. J Magn Reson Imaging. 2002; 15(6):693–704. PubMed PMID: 12112520. [PubMed: 12112520]
7. Englander SA, Ulug AM, Brem R, Glickson JD, van Zijl PC. Diffusion imaging of human breast. NMR Biomed. 1997; 10(7):348–352. Epub 1998/02/21. PubMed PMID: 9471126. [PubMed: 9471126]
8. Le Bihan D, Poupon C, Amadon A, Lethimonnier F. Artifacts and pitfalls in diffusion MRI. J Magn Reson Imaging. 2006; 24(3):478–488. Epub 2006/08/10. PubMed PMID: 16897692. [PubMed: 16897692]
9. Baron P, Dorrius MD, Kappert P, Oudkerk M, Sijens PE. Diffusion-weighted imaging of normal fibroglandular breast tissue: influence of microperfusion and fat suppression technique on the apparent diffusion coefficient. NMR in Biomedicine. 2010; 23(4):399–405. [PubMed: 20131313]

10. Partridge SC, Singer L, Sun R, Wilmes LJ, Klifa CS, Lehman CD, et al. Diffusion-weighted MRI: influence of intravoxel fat signal and breast density on breast tumor conspicuity and apparent diffusion coefficient measurements. Magn Reson Imaging. 2011; 29(9):1215–1221. PubMed PMID: 21920686; PubMed Central PMCID: PMC3199288. [PubMed: 21920686]
11. Bammer R, Keeling SL, Augustin M, Pruessmann KP, Wolf R, Stollberger R, et al. Improved diffusion-weighted single-shot echo-planar imaging (EPI) in stroke using sensitivity encoding (SENSE). Magn Reson Med. 2001; 46(3):548–554. Epub 2001/09/11. PubMed PMID: 11550248. [PubMed: 11550248]
12. Kuhl CK, Gieseke J, von Falkenhausen M, Textor J, Gernert S, Sonntag C, et al. Sensitivity encoding for diffusion-weighted MR imaging at 3.0 T: intraindividual comparative study. Radiology. 2005; 234(2):517–526. Epub 2005/01/27. PubMed PMID: 15671005. [PubMed: 15671005]
13. Bogner W, Gruber S, Pinker K, Grabner G, Stadlbauer A, Weber M, et al. Diffusion-weighted MR for differentiation of breast lesions at 3.0 T: how does selection of diffusion protocols affect diagnosis? Radiology. 2009; 253(2):341–351. Epub 2009/08/26. PubMed PMID: 19703869. [PubMed: 19703869]
14. Teruel JR, Fjosne HE, Ostlie A, Holland D, Dale AM, Bathen TF, et al. Inhomogeneous static magnetic field-induced distortion correction applied to diffusion weighted MRI of the breast at 3T. Magn Reson Med. 2014 PubMed PMID: 25323982.
15. Arlinghaus LR, Welch EB, Chakravarthy AB, Xu L, Farley JS, Abramson VG, et al. Motion correction in diffusion-weighted MRI of the breast at 3T. J Magn Reson Imaging. 2011; 33(5): 1063–1070. Epub 2011/04/22. PubMed PMID: 21509862; PubMed Central PMCID: PMC3081111. [PubMed: 21509862]
16. Veeraraghavan H, Do RK, Reidy DL, Deasy JO. Simultaneous segmentation and iterative registration method for computing ADC with reduced artifacts from DW-MRI. Med Phys. 2015; 42(5):2249–2260. Epub 2015/05/17. PubMed PMID: 25979019. [PubMed: 25979019]
17. Partridge SC, DeMartini WB, Kurland BF, Eby PR, White SW, Lehman CD. Quantitative diffusion-weighted imaging as an adjunct to conventional breast MRI for improved positive predictive value. AJR Am J Roentgenol. 2009; 193(6):1716–1722. PubMed PMID: 19933670. [PubMed: 19933670]
18. Chen X, Li WL, Zhang YL, Wu Q, Guo YM, Bai ZL. Meta-analysis of quantitative diffusion-weighted MR imaging in the differential diagnosis of breast lesions. BMC Cancer. 2010; 10:693. PubMed PMID: 21189150; PubMed Central PMCID: PMC3024311. [PubMed: 21189150]
19. Zhang L, Tang M, Min Z, Lu J, Lei X, Zhang X. Accuracy of combined dynamic contrast-enhanced magnetic resonance imaging and diffusion-weighted imaging for breast cancer detection: a meta-analysis. Acta Radiol. 2016; 57(6):651–660. Epub 2015/08/16. PubMed PMID: 26275624. [PubMed: 26275624]
20. Bickelhaupt S, Laun FB, Tesdorff J, Lederer W, Daniel H, Stieber A, et al. Fast and Noninvasive Characterization of Suspicious Lesions Detected at Breast Cancer X-Ray Screening: Capability of Diffusion-weighted MR Imaging with MIPs. Radiology. 2015:150425. PubMed PMID: 26418516.
21. Peters NH, Vincken KL, van den Bosch MA, Luijten PR, Mali WP, Bartels LW. Quantitative diffusion weighted imaging for differentiation of benign and malignant breast lesions: the influence of the choice of b-values. J Magn Reson Imaging. 2010; 31(5):1100–1105. Epub 2010/05/01. PubMed PMID: 20432344. [PubMed: 20432344]
22. Dorrius MD, Dijkstra H, Oudkerk M, Sijens PE. Effect of b value and pre-admission of contrast on diagnostic accuracy of 1.5-T breast DWI: a systematic review and meta-analysis. Eur Radiol. 2014; 24(11):2835–2847. PubMed PMID: 25103535. [PubMed: 25103535]
23. Choi SY, Chang YW, Park HJ, Kim HJ, Hong SS, Seo DY. Correlation of the apparent diffusion coefficiency values on diffusion-weighted imaging with prognostic factors for breast cancer. The British journal of radiology. 2012; 85(1016):e474–e479. Epub 2011/12/01. PubMed PMID: 22128125; PubMed Central PMCID: PMC3587081. [PubMed: 22128125]
24. Kim EJ, Kim SH, Park GE, Kang BJ, Song BJ, Kim YJ, et al. Histogram analysis of apparent diffusion coefficient at 3.0t: Correlation with prognostic factors and subtypes of invasive ductal carcinoma. J Magn Reson Imaging. 2015; 42(6):1666–1678. Epub 2015/04/29. PubMed PMID: 25919239. [PubMed: 25919239]

25. Kitajima K, Yamano T, Fukushima K, Miyoshi Y, Hirota S, Kawanaka Y, et al. Correlation of the SUVmax of FDG-PET and ADC values of diffusion-weighted MR imaging with pathologic prognostic factors in breast carcinoma. European journal of radiology. 2016; 85(5):943–949. Epub 2016/05/01. PubMed PMID: 27130054. [PubMed: 27130054]
26. Mori N, Ota H, Mugikura S, Takasawa C, Ishida T, Watanabe G, et al. Luminal-type breast cancer: correlation of apparent diffusion coefficients with the Ki-67 labeling index. Radiology. 2015; 274(1):66–73. Epub 2014/09/10. PubMed PMID: 25203132. [PubMed: 25203132]
27. Jiang R, Ma Z, Dong H, Sun S, Zeng X, Li X. Diffusion tensor imaging of breast lesions: evaluation of apparent diffusion coefficient and fractional anisotropy and tissue cellularity. The British journal of radiology. 2016; 89(1064):20160076. Epub 2016/06/16. PubMed PMID: 27302492. [PubMed: 27302492]
28. Costantini M, Belli P, Rinaldi P, Bufi E, Giardina G, Franceschini G, et al. Diffusion-weighted imaging in breast cancer: relationship between apparent diffusion coefficient and tumour aggressiveness. Clin Radiol. 2010; 65(12):1005–1012. PubMed PMID: 21070905. [PubMed: 21070905]
29. Razek AA, Gaballa G, Denewer A, Nada N. Invasive ductal carcinoma: correlation of apparent diffusion coefficient value with pathological prognostic factors. NMR Biomed. 2010; 23(6):619–623. PubMed PMID: 20232453. [PubMed: 20232453]
30. Park SH, Choi HY, Hahn SY. Correlations between apparent diffusion coefficient values of invasive ductal carcinoma and pathologic factors on diffusion-weighted MRI at 3.0 Tesla. J Magn Reson Imaging. 2015; 41(1):175–182. Epub 2013/12/20. PubMed PMID: 24353241. [PubMed: 24353241]
31. Guvenc I, Akay S, Ince S, Yildiz R, Kilbas Z, Oysul FG, et al. Apparent diffusion coefficient value in invasive ductal carcinoma at 3.0 Tesla: is it correlated with prognostic factors? The British journal of radiology. 2016; 89(1060):20150614. Epub 2016/02/09. PubMed PMID: 26853508; PubMed Central PMCID: PMC4846196. [PubMed: 26853508]
32. Jeh SK, Kim SH, Kim HS, Kang BJ, Jeong SH, Yim HW, et al. Correlation of the apparent diffusion coefficient value and dynamic magnetic resonance imaging findings with prognostic factors in invasive ductal carcinoma. J Magn Reson Imaging. 2011; 33(1):102–109. PubMed PMID: 21182127. [PubMed: 21182127]
33. Kamitani T, Matsuo Y, Yabuuchi H, Fujita N, Nagao M, Jinnouchi M, et al. Correlations between apparent diffusion coefficient values and prognostic factors of breast cancer. Magn Reson Med Sci. 2013; 12(3):193–199. Epub 2013/07/17. PubMed PMID: 23857151. [PubMed: 23857151]
34. Kim SH, Cha ES, Kim HS, Kang BJ, Choi JJ, Jung JH, et al. Diffusion-weighted imaging of breast cancer: correlation of the apparent diffusion coefficient value with prognostic factors. J Magn Reson Imaging. 2009; 30(3):615–620. Epub 2009/08/28. PubMed PMID: 19711411. [PubMed: 19711411]
35. Martincich L, Deantoni V, Bertotto I, Redana S, Kubatzki F, Sarotto I, et al. Correlations between diffusion-weighted imaging and breast cancer biomarkers. Eur Radiol. 2012; 22(7):1519–1528. PubMed PMID: 22411304. [PubMed: 22411304]
36. Rahbar H, Partridge SC, Eby PR, Demartini WB, Gutierrez RL, Peacock S, et al. Characterization of ductal carcinoma in situ on diffusion weighted breast MRI. Eur Radiol. 2011; 21(9):2011–2019. Epub 2011/05/13. PubMed PMID: 21562806. [PubMed: 21562806]
37. Bickel H, Pinker-Domenig K, Bogner W, Spick C, Bago-Horvath Z, Weber M, et al. Quantitative apparent diffusion coefficient as a noninvasive imaging biomarker for the differentiation of invasive breast cancer and ductal carcinoma in situ. Investigative radiology. 2015; 50(2):95–100. Epub 2014/10/22. PubMed PMID: 25333308. [PubMed: 25333308]
38. Hussein H, Chung C, Moshonov H, Miller N, Kulkarni SR, Scaranelo AM. Evaluation of Apparent Diffusion Coefficient to Predict Grade, Microinvasion, and Invasion in Ductal Carcinoma In Situ of the Breast. Academic radiology. 2015; 22(12):1483–1488. Epub 2015/09/24. PubMed PMID: 26391856. [PubMed: 26391856]
39. Mori N, Ota H, Mugikura S, Takasawa C, Tominaga J, Ishida T, et al. Detection of invasive components in cases of breast ductal carcinoma in situ on biopsy by using apparent diffusion coefficient MR parameters. Eur Radiol. 2013; 23(10):2705–2712. Epub 2013/06/05. PubMed PMID: 23732688. [PubMed: 23732688]

40. Iima M, Le Bihan D, Okumura R, Okada T, Fujimoto K, Kanao S, et al. Apparent diffusion coefficient as an MR imaging biomarker of low-risk ductal carcinoma in situ: a pilot study. Radiology. 2011; 260(2):364–372. Epub 2011/06/03. PubMed PMID: 21633054. [PubMed: 21633054]
41. Rahbar H, Partridge SC, Demartini WB, Gutierrez RL, Allison KH, Peacock S, et al. In vivo assessment of ductal carcinoma in situ grade: a model incorporating dynamic contrast-enhanced and diffusion-weighted breast MR imaging parameters. Radiology. 2012; 263(2):374–382. PubMed PMID: 22517955; PubMed Central PMCID: PMC3329273. [PubMed: 22517955]
42. Xing H, Song CL, Li WJ. Meta analysis of lymph node metastasis of breast cancer patients: Clinical value of DWI and ADC value. European journal of radiology. 2016; 85(6):1132–1137. Epub 2016/05/11. PubMed PMID: 27161063. [PubMed: 27161063]
43. Rahbar H, Conlin JL, Parsian S, DeMartini WB, Peacock S, Lehman CD, et al. Suspicious axillary lymph nodes identified on clinical breast MRI in patients newly diagnosed with breast cancer: can quantitative features improve discrimination of malignant from benign? Acad Radiol. 2015; 22(4): 430–438. Epub 2014/12/11. PubMed PMID: 25491740; PubMed Central PMCID: PMC4355079. [PubMed: 25491740]
44. Iima M, Kataoka M, Okumura R, Togashi K. Detection of axillary lymph node metastasis with diffusion-weighted MR imaging. Clin Imaging. 2014; 38(5):633–636. Epub 2014/06/09. PubMed PMID: 24908365. [PubMed: 24908365]
45. Galban CJ, Ma B, Malyarenko D, Pickles MD, Heist K, Henry NL, et al. Multi-site clinical evaluation of DW-MRI as a treatment response metric for breast cancer patients undergoing neoadjuvant chemotherapy. PLoS One. 2015; 10(3):e0122151. Epub 2015/03/31. PubMed PMID: 25816249; PubMed Central PMCID: PMC4376686. [PubMed: 25816249]
46. Li XR, Cheng LQ, Liu M, Zhang YJ, Wang JD, Zhang AL, et al. DW-MRI ADC values can predict treatment response in patients with locally advanced breast cancer undergoing neoadjuvant chemotherapy. Med Oncol. 2012; 29(2):425–431. Epub 2011/02/03. PubMed PMID: 21286861. [PubMed: 21286861]
47. Sharma U, Danishad KK, Seenu V, Jagannathan NR. Longitudinal study of the assessment by MRI and diffusion-weighted imaging of tumor response in patients with locally advanced breast cancer undergoing neoadjuvant chemotherapy. NMR Biomed. 2009; 22(1):104–113. PubMed PMID: 18384182. [PubMed: 18384182]
48. Richard R, Thomassin I, Chapellier M, Scemama A, de Cremoux P, Varna M, et al. Diffusion-weighted MRI in pretreatment prediction of response to neoadjuvant chemotherapy in patients with breast cancer. Eur Radiol. 2013; 23(9):2420–2431. PubMed PMID: 23652844. [PubMed: 23652844]
49. Liu S, Ren R, Chen Z, Wang Y, Fan T, Li C, et al. Diffusion-weighted imaging in assessing pathological response of tumor in breast cancer subtype to neoadjuvant chemotherapy. J Magn Reson Imaging. 2015; 42(3):779–787. Epub 2015/01/13. PubMed PMID: 25580585. [PubMed: 25580585]
50. Bufi E, Belli P, Costantini M, Cipriani A, Di Matteo M, Bonatesta A, et al. Role of the Apparent Diffusion Coefficient in the Prediction of Response to Neoadjuvant Chemotherapy in Patients With Locally Advanced Breast Cancer. Clin Breast Cancer. 2015; 15(5):370–380. Epub 2015/04/22. PubMed PMID: 25891905. [PubMed: 25891905]
51. Kazama T, Kuroki Y, Kikuchi M, Sato Y, Nagashima T, Miyazawa Y, et al. Diffusion-weighted MRI as an adjunct to mammography in women under 50 years of age: an initial study. J Magn Reson Imaging. 2012; 36(1):139–144. PubMed PMID: 22359367. [PubMed: 22359367]
52. Trimboli RM, Verardi N, Cartia F, Carbonaro LA, Sardanelli F. Breast cancer detection using double reading of unenhanced MRI including T1-weighted, T2-weighted STIR, and diffusion-weighted imaging: a proof of concept study. AJR Am J Roentgenol. 2014; 203(3):674–681. PubMed PMID: 25148175. [PubMed: 25148175]
53. Yabuuchi H, Matsuo Y, Sunami S, Kamitani T, Kawanami S, Setoguchi T, et al. Detection of non-palpable breast cancer in asymptomatic women by using unenhanced diffusion-weighted and T2-weighted MR imaging: comparison with mammography and dynamic contrast-enhanced MR imaging. Eur Radiol. 2011; 21(1):11–17. PubMed PMID: 20640898. [PubMed: 20640898]

54. McDonald ES, Hammersley JA, Chou SS, Rahbar H, Scheel JR, Lee CI, et al. Performance of DWI as a Rapid Unenhanced Technique for Detecting Mammographically Occult Breast Cancer in Elevated-Risk Women With Dense Breasts. AJR Am J Roentgenol. 2016:W1–W12. PubMed PMID: 27077731.
55. Partridge SC, Demartini WB, Kurland BF, Eby PR, White SW, Lehman CD. Differential diagnosis of mammographically and clinically occult breast lesions on diffusion-weighted MRI. J Magn Reson Imaging. 2010; 31(3):562–570. PubMed PMID: 20187198. [PubMed: 20187198]
56. O'Flynn EA, Blackledge M, Collins D, Downey K, Doran S, Patel H, et al. Evaluating the diagnostic sensitivity of computed diffusion-weighted MR imaging in the detection of breast cancer. J Magn Reson Imaging. 2016 Epub 2016/01/15. PubMed PMID: 26762608.
57. Tamura T, Murakami S, Naito K, Yamada T, Fujimoto T, Kikkawa T. Investigation of the optimal b-value to detect breast tumors with diffusion weighted imaging by 1.5-T MRI. Cancer Imaging. 2014; 14:11. Epub 2015/01/23. PubMed PMID: 25608450; PubMed Central PMCID: PMC4331817. [PubMed: 25608450]
58. Ray KM, Price ER, Joe BN. Breast density legislation: mandatory disclosure to patients, alternative screening, billing, reimbursement. AJR Am J Roentgenol. 2015; 204(2):257–260. Epub 2015/01/24. PubMed PMID: 25615746. [PubMed: 25615746]
59. Slanetz PJ, Freer PE, Birdwell RL. Breast-density legislation--practical considerations. N Engl J Med. 2015; 372(7):593–595. Epub 2015/02/12. PubMed PMID: 25671249. [PubMed: 25671249]
60. Kanal E, Tweedle MF. Residual or retained gadolinium: practical implications for radiologists and our patients. Radiology. 2015; 275(3):630–634. PubMed PMID: 25942418. [PubMed: 25942418]
61. Vogel PM, Georgiade NG, Fetter BF, Vogel FS, McCarty KS Jr. The correlation of histologic changes in the human breast with the menstrual cycle. Am J Pathol. 1981; 104(1):23–34. PubMed PMID: 7258295; PubMed Central PMCID: PMC1903738. [PubMed: 7258295]
62. Weinstein SP, Conant EF, Sehgal CM, Woo IP, Patton JA. Hormonal variations in the vascularity of breast tissue. J Ultrasound Med. 2005; 24(1):67–72. quiz 4. PubMed PMID: 15615930. [PubMed: 15615930]
63. Kuhl CK, Bieling HB, Gieseke J, Kreft BP, Sommer T, Lutterbey G, et al. Healthy premenopausal breast parenchyma in dynamic contrast-enhanced MR imaging of the breast: normal contrast medium enhancement and cyclical-phase dependency. Radiology. 1997; 203(1):137–144. PubMed PMID: 9122382. [PubMed: 9122382]
64. Muller-Schimpfle M, Ohmenhauser K, Stoll P, Dietz K, Claussen CD. Menstrual cycle and age: influence on parenchymal contrast medium enhancement in MR imaging of the breast. Radiology. 1997; 203(1):145–149. PubMed PMID: 9122383. [PubMed: 9122383]
65. Ramakrishnan R, Khan SA, Badve S. Morphological changes in breast tissue with menstrual cycle. Mod Pathol. 2002; 15(12):1348–1356. PubMed PMID: 12481017. [PubMed: 12481017]
66. White E, Velentgas P, Mandelson MT, Lehman CD, Elmore JG, Porter P, et al. Variation in mammographic breast density by time in menstrual cycle among women aged 40-49 years. J Natl Cancer Inst. 1998; 90(12):906–910. PubMed PMID: 9637139. [PubMed: 9637139]
67. Miglioretti DL, Walker R, Weaver DL, Buist DS, Taplin SH, Carney PA, et al. Accuracy of screening mammography varies by week of menstrual cycle. Radiology. 2011; 258(2):372–379. PubMed PMID: 21131584; PubMed Central PMCID: PMC3029886. [PubMed: 21131584]
68. Partridge SC, McKinnon GC, Henry RG, Hylton NM. Menstrual cycle variation of apparent diffusion coefficients measured in the normal breast using MRI. Journal of Magnetic Resonance Imaging. 2001; 14(4):433–438. Epub 2001/10/13. PubMed PMID: 11599068. [PubMed: 11599068]
69. O'Flynn EA, Morgan VA, Giles SL, deSouza NM. Diffusion weighted imaging of the normal breast: reproducibility of apparent diffusion coefficient measurements and variation with menstrual cycle and menopausal status. Eur Radiol. 2012; 22(7):1512–1518. PubMed PMID: 22367471. [PubMed: 22367471]
70. Kim JY, Suh HB, Kang HJ, Shin JK, Choo KS, Nam KJ, et al. Apparent diffusion coefficient of breast cancer and normal fibroglandular tissue in diffusion-weighted imaging: the effects of menstrual cycle and menopausal status. Breast cancer research and treatment. 2016; 157(1):31–40. Epub 2016/04/20. PubMed PMID: 27091644. [PubMed: 27091644]

71. Nissan N, Furman-Haran E, Shapiro-Feinberg M, Grobgeld D, Degani H. Diffusion-tensor MR imaging of the breast: hormonal regulation. Radiology. 2014; 271(3):672–680. PubMed PMID: 24533873. [PubMed: 24533873]

72. Shin S, Ko ES, Kim RB, Han BK, Nam SJ, Shin JH, et al. Effect of menstrual cycle and menopausal status on apparent diffusion coefficient values and detectability of invasive ductal carcinoma on diffusion-weighted MRI. Breast cancer research and treatment. 2015; 149(3):751–759. PubMed PMID: 25638396. [PubMed: 25638396]

73. Clendenen TV, Kim S, Moy L, Wan L, Rusinek H, Stanczyk FZ, et al. Magnetic resonance imaging (MRI) of hormone-induced breast changes in young premenopausal women. Magn Reson Imaging. 2013; 31(1):1–9. PubMed PMID: 22898693. [PubMed: 22898693]

74. McDonald ES, Schopp JG, Peacock S, DeMartini WB, Rahbar H, Lehman CD, et al. Diffusion-weighted MRI: association between patient characteristics and apparent diffusion coefficients of normal breast fibroglandular tissue at 3 T. AJR Am J Roentgenol. 2014; 202(5):W496–W502. Epub 2014/04/25. PubMed PMID: 24758685; PubMed Central PMCID: PMC4080610. [PubMed: 24758685]

75. Iacconi C, Thakur SB, Dershaw DD, Brooks J, Fry CW, Morris EA. Impact of fibroglandular tissue and background parenchymal enhancement on diffusion weighted imaging of breast lesions. European journal of radiology. 2014; 83(12):2137–2143. PubMed PMID: 25445896. [PubMed: 25445896]

76. Cho GY, Moy L, Kim SG, Klautau Leite AP, Baete SH, Babb JS, et al. Comparison of contrast enhancement and diffusion-weighted magnetic resonance imaging in healthy and cancerous breast tissue. European journal of radiology. 2015; 84(10):1888–1893. PubMed PMID: 26220915. [PubMed: 26220915]

77. Plaza MJ, Morris EA, Thakur SB. Diffusion tensor imaging in the normal breast: influences of fibroglandular tissue composition and background parenchymal enhancement. Clin Imaging. 2016; 40(3):506–511. PubMed PMID: 27133695; PubMed Central PMCID: PMC4853756. [PubMed: 27133695]

78. Espinosa LA, Daniel BL, Vidarsson L, Zakhour M, Ikeda DM, Herfkens RJ. The lactating breast: contrast-enhanced MR imaging of normal tissue and cancer. Radiology. 2005; 237(2):429–436. PubMed PMID: 16244250. [PubMed: 16244250]

79. Neville MC, McFadden TB, Forsyth I. Hormonal regulation of mammary differentiation and milk secretion. J Mammary Gland Biol Neoplasia. 2002; 7(1):49–66. PubMed PMID: 12160086. [PubMed: 12160086]

80. Neville MC, Allen JC, Archer PC, Casey CE, Seacat J, Keller RP, et al. Studies in human lactation: milk volume and nutrient composition during weaning and lactogenesis. Am J Clin Nutr. 1991; 54(1):81–92. PubMed PMID: 2058592. [PubMed: 2058592]

81. Sah RG, Agarwal K, Sharma U, Parshad R, Seenu V, Jagannathan NR. Characterization of malignant breast tissue of breast cancer patients and the normal breast tissue of healthy lactating women volunteers using diffusion MRI and in vivo 1H MR spectroscopy. J Magn Reson Imaging. 2015; 41(1):169–174. PubMed PMID: 24273108. [PubMed: 24273108]

82. Ei Khouli RH, Jacobs MA, Mezban SD, Huang P, Kamel IR, Macura KJ, et al. Diffusion-weighted imaging improves the diagnostic accuracy of conventional 3.0-T breast MR imaging. Radiology. 2010; 256(1):64–73. PubMed PMID: 20574085; PubMed Central PMCID: PMC2897691. [PubMed: 20574085]

83. Bogner W, Pinker-Domenig K, Bickel H, Chmelik M, Weber M, Helbich TH, et al. Readout-segmented echo-planar imaging improves the diagnostic performance of diffusion-weighted MR breast examinations at 3.0 T. Radiology. 2012; 263(1):64–76. PubMed PMID: 22438442. [PubMed: 22438442]

84. Wisner DJ, Rogers N, Deshpande VS, Newitt DN, Laub GA, Porter DA, et al. High-resolution diffusion-weighted imaging for the separation of benign from malignant BI-RADS 4/5 lesions found on breast MRI at 3T. J Magn Reson Imaging. 2014; 40(3):674–681. Epub 2013/11/12. PubMed PMID: 24214467; PubMed Central PMCID: PMC4014534. [PubMed: 24214467]

85. Filli L, Ghafoor S, Kenkel D, Liu W, Weiland E, Andreisek G, et al. Simultaneous multi-slice readout-segmented echo planar imaging for accelerated diffusion-weighted imaging of the breast.

European journal of radiology. 2016; 85(1):274–278. PubMed PMID: 26547123. [PubMed: 26547123]

86. Kim YJ, Kim SH, Kang BJ, Park CS, Kim HS, Son YH, et al. Readout-segmented echo-planar imaging in diffusion-weighted mr imaging in breast cancer: comparison with single-shot echo-planar imaging in image quality. Korean J Radiol. 2014; 15(4):403–410. PubMed PMID: 25053898; PubMed Central PMCID: PMCPMC4105801. [PubMed: 25053898]
87. Dong H, Li Y, Yu K, Li H. Comparison of image quality and application values on different field-of-view diffusion-weighted imaging of breast cancer. Acta Radiol. 2016; 57(1):19–24. PubMed PMID: 25638799. [PubMed: 25638799]
88. Park JY, Shin HJ, Shin KC, Sung YS, Choi WJ, Chae EY, et al. Comparison of readout segmented echo planar imaging (EPI) and EPI with reduced field-of-VIew diffusion-weighted imaging at 3t in patients with breast cancer. J Magn Reson Imaging. 2015; 42(6):1679–1688. PubMed PMID: 25946597. [PubMed: 25946597]
89. Barentsz MW, Taviani V, Chang JM, Ikeda DM, Miyake KK, Banerjee S, et al. Assessment of tumor morphology on diffusion-weighted (DWI) breast MRI: Diagnostic value of reduced field of view DWI. J Magn Reson Imaging. 2015; 42(6):1656–1665. PubMed PMID: 25914178; PubMed Central PMCID: PMCPMC4619182. [PubMed: 25914178]
90. McLaughlin RL, Newitt DC, Wilmes LJ, Jones EF, Wisner DJ, Kornak J, et al. High resolution in vivo characterization of apparent diffusion coefficient at the tumor-stromal boundary of breast carcinomas: a pilot study to assess treatment response using proximity-dependent diffusion-weighted imaging. J Magn Reson Imaging. 2014; 39(5):1308–1313. PubMed PMID: 24719242; PubMed Central PMCID: PMCPMC3983569. [PubMed: 24719242]
91. Alsop DC. Phase insensitive preparation of single-shot RARE: Application to diffusion imaging in humans. Magnetic Resonance in Medicine. 1997; 38(4):527–533. [PubMed: 9324317]
92. Norris DG. Selective parity RARE imaging. Magnetic Resonance in Medicine. 2007; 58(4):643–649. [PubMed: 17899602]
93. Williams CFM, Redpath TW, Norris DG. A novel fast split-echo multi-shot diffusion-weighted MRI method using navigator echoes. Magnetic Resonance in Medicine. 1999; 41(4):734–742. PubMed PMID: ISI:000081422200012. [PubMed: 10332849]
94. Le Roux P. Non-CPMG fast spin echo with full signal. Journal of Magnetic Resonance. 2002; 155(2):278–292. PubMed PMID: ISI:000176073700009. [PubMed: 12036339]
95. Baltzer PAT, Renz DM, Herrmann KH, Dietzel M, Krumbein I, Gajda M, et al. Diffusion-weighted imaging (DWI) in MR mammography (MRM): clinical comparison of echo planar imaging (EPI) and half-Fourier single-shot turbo spin echo (HASTE) diffusion techniques. European Radiology. 2009; 19(7):1612–1620. PubMed PMID: ISI:000266780800006. [PubMed: 19288109]
96. Cho GY, Moy L, Kim SG, Baete SH, Moccaldi M, Babb JS, et al. Evaluation of breast cancer using intravoxel incoherent motion (IVIM) histogram analysis: comparison with malignant status, histological subtype, and molecular prognostic factors. Eur Radiol. 2015 PubMed PMID: 26615557.
97. Lo GG, Ai V, Chan JKF, Li KW, Cheung PSY, Wong TT, et al. Diffusion-Weighted Magnetic Resonance Imaging of Breast Lesions: First Experiences at 3 T. Journal of Computer Assisted Tomography. 2009; 33(1):63–69. PubMed PMID: ISI:000263135900011. [PubMed: 19188787]
98. Kinoshita T, Yashiro N, Ihara N, Funatu H, Fukuma E, Narita M. Diffusion-weighted half-fourier single-shot turbo spin echo imaging in breast tumors: Differentiation of invasive ductal carcinoma from fibroadenoma. Journal of Computer Assisted Tomography. 2002; 26(6):1042–1046. PubMed PMID: ISI:000180051700033. [PubMed: 12488758]
99. Miller KL, Pauly JM. Nonlinear phase correction for navigated diffusion imaging. Magnetic Resonance in Medicine. 2003; 50(2):343–353. [PubMed: 12876711]
100. Wu EX, Buxton RB. Effect of Diffusion on the Steady-State Magnetization with Pulsed Field Gradients. Journal of Magnetic Resonance. 1990; 90(2):243–253.
101. Granlund KL, Staroswiecki E, Alley MT, Daniel BL, Hargreaves BA. High-resolution, three-dimensional diffusion-weighted breast imaging using DESS. Magn Reson Imaging. 2014; 32(4): 330–341. PubMed PMID: 24512800; PubMed Central PMCID: PMCPMC4041802. [PubMed: 24512800]

102. Solomon E, Nissan N, Furman-Haran E, Seginer A, Shapiro-Feinberg M, Degani H, et al. Overcoming limitations in diffusion-weighted MRI of breast by spatio-temporal encoding. Magn Reson Med. 2015; 73(6):2163–2173. PubMed PMID: 25045867. [PubMed: 25045867]
103. Schmitz AM, Veldhuis WB, Menke-Pluijmers MB, van der Kemp WJ, van der Velden TA, Kock MC, et al. Multiparametric MRI With Dynamic Contrast Enhancement, Diffusion-Weighted Imaging, and 31-Phosphorus Spectroscopy at 7 T for Characterization of Breast Cancer. Investigative radiology. 2015; 50(11):766–771. PubMed PMID: 26135017. [PubMed: 26135017]
104. Pinker K, Baltzer P, Bogner W, Leithner D, Trattnig S, Zaric O, et al. Multiparametric MR Imaging with High-Resolution Dynamic Contrast-enhanced and Diffusion-weighted Imaging at 7 T Improves the Assessment of Breast Tumors: A Feasibility Study. Radiology. 2015; 276(2):360–370. PubMed PMID: 25751227. [PubMed: 25751227]
105. Bogner W, Pinker K, Zaric O, Baltzer P, Minarikova L, Porter D, et al. Bilateral diffusion-weighted MR imaging of breast tumors with submillimeter resolution using readout-segmented echo-planar imaging at 7 T. Radiology. 2015; 274(1):74–84. PubMed PMID: 25341078. [PubMed: 25341078]
106. Gruber S, Minarikova L, Pinker K, Zaric O, Chmelik M, Strasser B, et al. Diffusion-weighted imaging of breast tumours at 3 Tesla and 7 Tesla: a comparison. Eur Radiol. 2015 PubMed PMID: 26310582.
107. Le Bihan D, Mangin JF, Poupon C, Clark CA, Pappata S, Molko N, et al. Diffusion tensor imaging: concepts and applications. J Magn Reson Imaging. 2001; 13(4):534–546. PubMed PMID: 11276097. [PubMed: 11276097]
108. Partridge SC, Murthy RS, Ziadloo A, White SW, Allison KH, Lehman CD. Diffusion tensor magnetic resonance imaging of the normal breast. Magn Reson Imaging. 2010; 28(3):320–328. PubMed PMID: 20061111. [PubMed: 20061111]
109. Tagliafico A, Rescinito G, Monetti F, Villa A, Chiesa F, Fisci E, et al. Diffusion tensor magnetic resonance imaging of the normal breast: reproducibility of DTI-derived fractional anisotropy and apparent diffusion coefficient at 3.0 T. Radiol Med. 2012; 117(6):992–1003. PubMed PMID: 22580812. [PubMed: 22580812]
110. Wiederer J, Pazahr S, Leo C, Nanz D, Boss A. Quantitative breast MRI: 2D histogram analysis of diffusion tensor parameters in normal tissue. MAGMA. 2014; 27(2):185–193. PubMed PMID: 23999995. [PubMed: 23999995]
111. Nissan N, Furman-Haran E, Feinberg-Shapiro M, Grobgeld D, Eyal E, Zehavi T, et al. Tracking the mammary architectural features and detecting breast cancer with magnetic resonance diffusion tensor imaging. J Vis Exp. 2014; (94) PubMed PMID: 25549209; PubMed Central PMCID: PMC4396944.
112. Partridge SC, Ziadloo A, Murthy R, White SW, Peacock S, Eby PR, et al. Diffusion tensor MRI: preliminary anisotropy measures and mapping of breast tumors. J Magn Reson Imaging. 2010; 31(2):339–347. PubMed PMID: 20099346. [PubMed: 20099346]
113. Tsougos I, Svolos P, Kousi E, Athanassiou E, Theodorou K, Arvanitis D, et al. The contribution of diffusion tensor imaging and magnetic resonance spectroscopy for the differentiation of breast lesions at 3T. Acta Radiol. 2014; 55(1):14–23. PubMed PMID: 23864060. [PubMed: 23864060]
114. Baltzer PA, Schafer A, Dietzel M, Grassel D, Gajda M, Camara O, et al. Diffusion tensor magnetic resonance imaging of the breast: a pilot study. Eur Radiol. 2011; 21(1):1–10. PubMed PMID: 20668860. [PubMed: 20668860]
115. Cakir O, Arslan A, Inan N, Anik Y, Sarisoy T, Gumustas S, et al. Comparison of the diagnostic performances of diffusion parameters in diffusion weighted imaging and diffusion tensor imaging of breast lesions. European journal of radiology. 2013; 82(12):e801–e806. PubMed PMID: 24099642. [PubMed: 24099642]
116. Eyal E, Shapiro-Feinberg M, Furman-Haran E, Grobgeld D, Golan T, Itzchak Y, et al. Parametric diffusion tensor imaging of the breast. Investigative radiology. 2012; 47(5):284–291. PubMed PMID: 22472798. [PubMed: 22472798]
117. Furman-Haran E, Grobgeld D, Nissan N, Shapiro-Feinberg M, Degani H. Can diffusion tensor anisotropy indices assist in breast cancer detection? J Magn Reson Imaging. 2016 PubMed PMID: 27092546.

118. Teruel JR, Goa PE, Sjobakk TE, Ostlie A, Fjosne HE, Bathen TF. Diffusion weighted imaging for the differentiation of breast tumors: From apparent diffusion coefficient to high order diffusion tensor imaging. J Magn Reson Imaging. 2016; 43(5):1111–1121. PubMed PMID: 26494124. [PubMed: 26494124]
119. Wang Y, Zhang X, Cao K, Li Y, Li X, Qi L, et al. Diffusion-tensor imaging as an adjunct to dynamic contrast-enhanced MRI for improved accuracy of differential diagnosis between breast ductal carcinoma in situ and invasive breast carcinoma. Chin J Cancer Res. 2015; 27(2):209–217. PubMed PMID: 25937784; PubMed Central PMCID: PMC4409968. [PubMed: 25937784]
120. Basser PJ, Pajevic S, Pierpaoli C, Duda J, Aldroubi A. In vivo fiber tractography using DT-MRI data. Magn Reson Med. 2000; 44(4):625–632. PubMed PMID: 11025519. [PubMed: 11025519]
121. Wang Y, Zhang XP, Li YL, Li XT, Hu Y, Cui Y, et al. Optimization of the parameters for diffusion tensor magnetic resonance imaging data acquisition for breast fiber tractography at 1.5 T. Clin Breast Cancer. 2014; 14(1):61–67. PubMed PMID: 24183417. [PubMed: 24183417]
122. Lebihan D, Breton E, Lallemand D, Aubin ML, Vignaud J, Lavaljeantet M. Separation of Diffusion and Perfusion in Intravoxel Incoherent Motion Mr Imaging. Radiology. 1988; 168(2): 497–505. PubMed PMID: WOS:A1988P303300037. [PubMed: 3393671]
123. Iima M, Le Bihan D. Clinical Intravoxel Incoherent Motion and Diffusion MR Imaging: Past, Present, and Future. Radiology. 2016; 278(1):13–32. PubMed PMID: 26690990. [PubMed: 26690990]
124. Sigmund EE, Cho GY, Kim S, Finn M, Moccaldi M, Jensen JH, et al. Intravoxel Incoherent Motion Imaging of Tumor Microenvironment in Locally Advanced Breast Cancer. Magnetic Resonance in Medicine. 2011; 65(5):1437–1447. PubMed PMID: ISI:000289760800030. [PubMed: 21287591]
125. Bokacheva L, Kaplan JB, Giri DD, Patil S, Gnanasigamani M, Nyman CG, et al. Intravoxel incoherent motion diffusion-weighted MRI at 3.0 T differentiates malignant breast lesions from benign lesions and breast parenchyma. J Magn Reson Imaging. 2014; 40(4):813–823. PubMed PMID: 24273096. [PubMed: 24273096]
126. Liu C, Liang C, Liu Z, Zhang S, Huang B. Intravoxel incoherent motion (IVIM) in evaluation of breast lesions: comparison with conventional DWI. European journal of radiology. 2013; 82(12):e782–e789. Epub 2013/09/17. PubMed PMID: 24034833. [PubMed: 24034833]
127. Iima M, Yano K, Kataoka M, Umehana M, Murata K, Kanao S, et al. Quantitative Non-Gaussian Diffusion and Intravoxel Incoherent Motion Magnetic Resonance Imaging: Differentiation of Malignant and Benign Breast Lesions. Investigative radiology. 2015; 50(4):205–211. PubMed PMID: 25260092. [PubMed: 25260092]
128. Suo S, Lin N, Wang H, Zhang L, Wang R, Zhang S, et al. Intravoxel incoherent motion diffusion-weighted MR imaging of breast cancer at 3.0 tesla: Comparison of different curve-fitting methods. J Magn Reson Imaging. 2015; 42(2):362–370. PubMed PMID: 25407944. [PubMed: 25407944]
129. Dijkstra H, Dorrius MD, Wielema M, Jaspers K, Pijnappel RM, Oudkerk M, et al. Semi-automated quantitative intravoxel incoherent motion analysis and its implementation in breast diffusion-weighted imaging. J Magn Reson Imaging. 2015 PubMed PMID: 26558851.
130. Panek R, Borri M, Orton M, O'Flynn E, Morgan V, Giles SL, et al. Evaluation of diffusion models in breast cancer. Med Phys. 2015; 42(8):4833–4839. PubMed PMID: 26233210. [PubMed: 26233210]
131. Kim Y, Ko K, Kim D, Min C, Kim SG, Joo J, et al. Intravoxel incoherent motion diffusion-weighted MR imaging of breast cancer: association with histopathological features and subtypes. The British journal of radiology. 2016:20160140. PubMed PMID: 27197744. [PubMed: 27197744]
132. Iima M, Yano K, Kataoka M, Umehana M, Murata K, Kanao S, et al. Quantitative non-Gaussian diffusion and intravoxel incoherent motion magnetic resonance imaging: differentiation of malignant and benign breast lesions. Investigative radiology. 2015; 50(4):205–211. Epub 2014/09/27. PubMed PMID: 25260092. [PubMed: 25260092]
133. Paran Y, Bendel P, Margalit R, Degani H. Water diffusion in the different microenvironments of breast cancer. Nmr in Biomedicine. 2004; 17(4):170–180. PubMed PMID: ISI: 000222810300002. [PubMed: 15229930]

134. Ko ES, Han BK, Kim RB, Cho EY, Ahn S, Nam SJ, et al. Apparent diffusion coefficient in estrogen receptor-positive invasive ductal breast carcinoma: correlations with tumor-stroma ratio. Radiology. 2014; 271(1):30–37. PubMed PMID: 24475830. [PubMed: 24475830]

135. Jensen JH, Helpern JA, Ramani A, Lu HZ, Kaczynski K. Diffusional kurtosis imaging: The quantification of non-Gaussian water diffusion by means of magnetic resonance imaging. Magnetic Resonance in Medicine. 2005; 53(6):1432–1440. PubMed PMID: ISI: 000229468200025. [PubMed: 15906300]

136. Sun K, Chen X, Chai W, Fei X, Fu C, Yan X, et al. Breast Cancer: Diffusion Kurtosis MR Imaging-Diagnostic Accuracy and Correlation with Clinical-Pathologic Factors. Radiology. 2015; 277(1):46–55. PubMed PMID: 25938679. [PubMed: 25938679]

137. Wu D, Li G, Zhang J, Chang S, Hu J, Dai Y. Characterization of breast tumors using diffusion kurtosis imaging (DKI). PLoS One. 2014; 9(11):e113240. PubMed PMID: 25406010; PubMed Central PMCID: PMCPMC4236178. [PubMed: 25406010]

138. Nogueira L, Brandao S, Matos E, Nunes RG, Loureiro J, Ramos I, et al. Application of the diffusion kurtosis model for the study of breast lesions. Eur Radiol. 2014; 24(6):1197–1203. PubMed PMID: 24658871. [PubMed: 24658871]

139. Fieremans E, Jensen JH, Helpern JA. White matter characterization with diffusional kurtosis imaging. NeuroImage. 2011; 58(1):177–188. Epub 2011/06/28. PubMed PMID: 21699989; PubMed Central PMCID: PMC3136876. [PubMed: 21699989]

140. Zhang H, Schneider T, Wheeler-Kingshott CA, Alexander DC. NODDI: practical in vivo neurite orientation dispersion and density imaging of the human brain. NeuroImage. 2012; 61(4):1000–1016. PubMed PMID: 22484410. [PubMed: 22484410]

141. Norddin N, Power C, Watson G, Cowin G, Kurniawan ND, Gluch L, et al. Microscopic diffusion properties of fixed breast tissue: Preliminary findings. Magn Reson Med. 2015; 74(6):1733–1739. PubMed PMID: 25522006. [PubMed: 25522006]

142. Novikov DS, Fieremans E, Jensen JH, Helpern JA. Random walks with barriers. Nature Physics. 2011; 7(6):508–514. PubMed PMID: WOS:000291146500021. [PubMed: 21686083]

143. Teruel JR, Cho GY, Moccaldi Rt M, Goa PE, Bathen TF, Feiweier T, et al. Stimulated echo diffusion tensor imaging (STEAM-DTI) with varying diffusion times as a probe of breast tissue. J Magn Reson Imaging. 2016 Epub 2016/07/22. PubMed PMID: 27441890.

144. American College of Radiology Imaging Network (ACRIN) 6702: A Multi-Center Study Evaluating the Utility of Diffusion Weighted Imaging for Detection and Diagnosis of Breast Cancer. [Accessed June 14, 2016] Available at: https://www.acrin.org/TabID/879/Default.aspx

145. American College of Radiology Imaging Network (ACRIN) 6698: Diffusion Weighted MR Imaging Biomarkers for Assessment of Breast Cancer Response to Neoadjuvant Treatment: A sub-study of the I-SPY 2 TRIAL (Investigation of Serial Studies to Predict Your Therapeutic Response with Imaging And moLecular Analysis). [Accessed June 14, 2016] Available at: https://www.acrin.org/TabID/825/Default.aspx

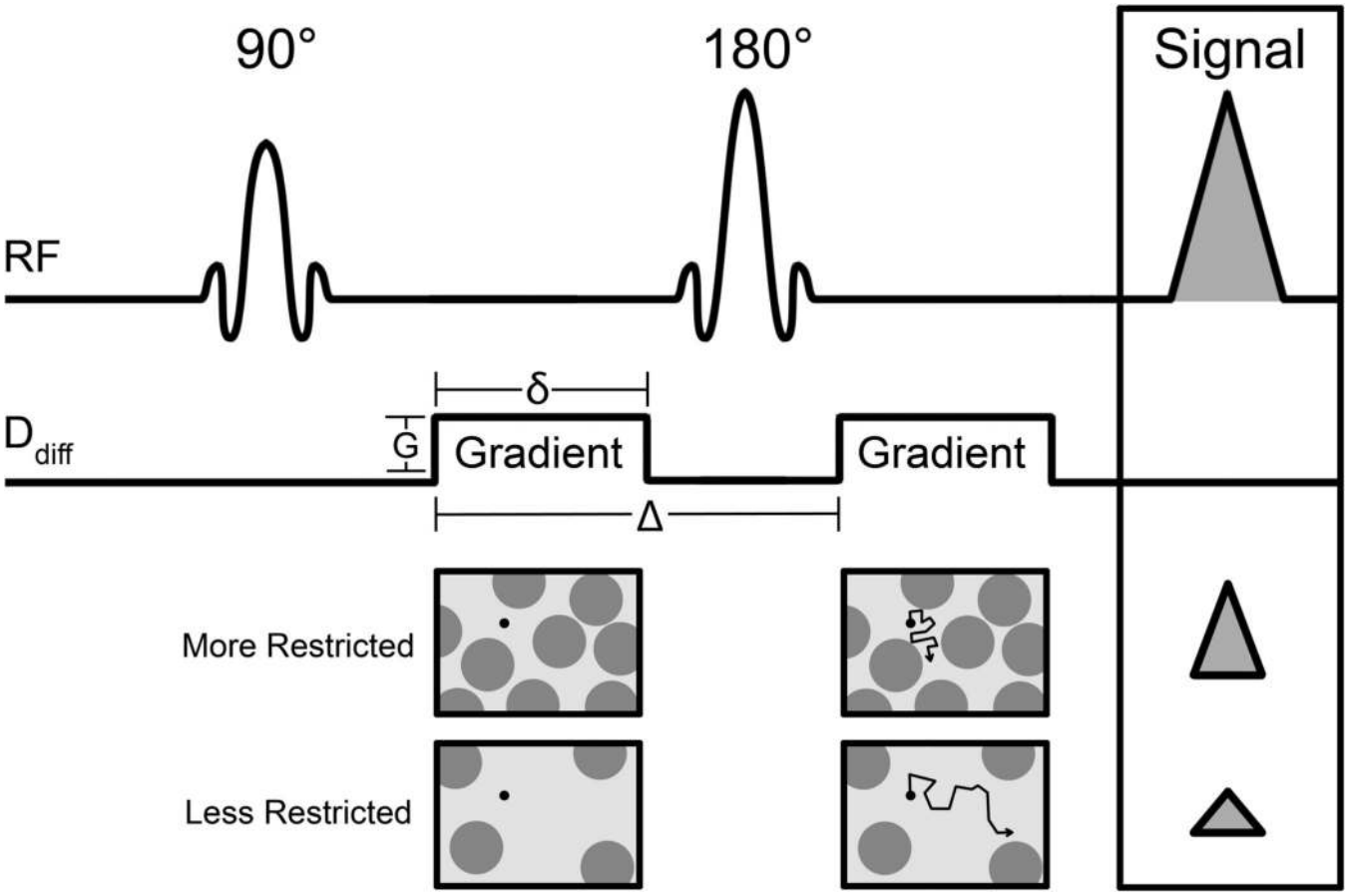

Figure 1.

Pulse-sequence diagram of a diffusion-weighted spin-echo sequence based on a Stejskal-Tanner encoding scheme. Two precisely matched diffusion-sensitizing gradients are inserted before and after a 180° radiofrequency refocusing pulse. Important factors defining the degree of diffusion sensitization ('b value') are the gradient amplitude (G), duration (δ), and the time between the two sensitizing gradients (Δ). The resulting signal is reduced in proportion to the water mobility, with less restricted environments exhibiting larger decreases in signal.

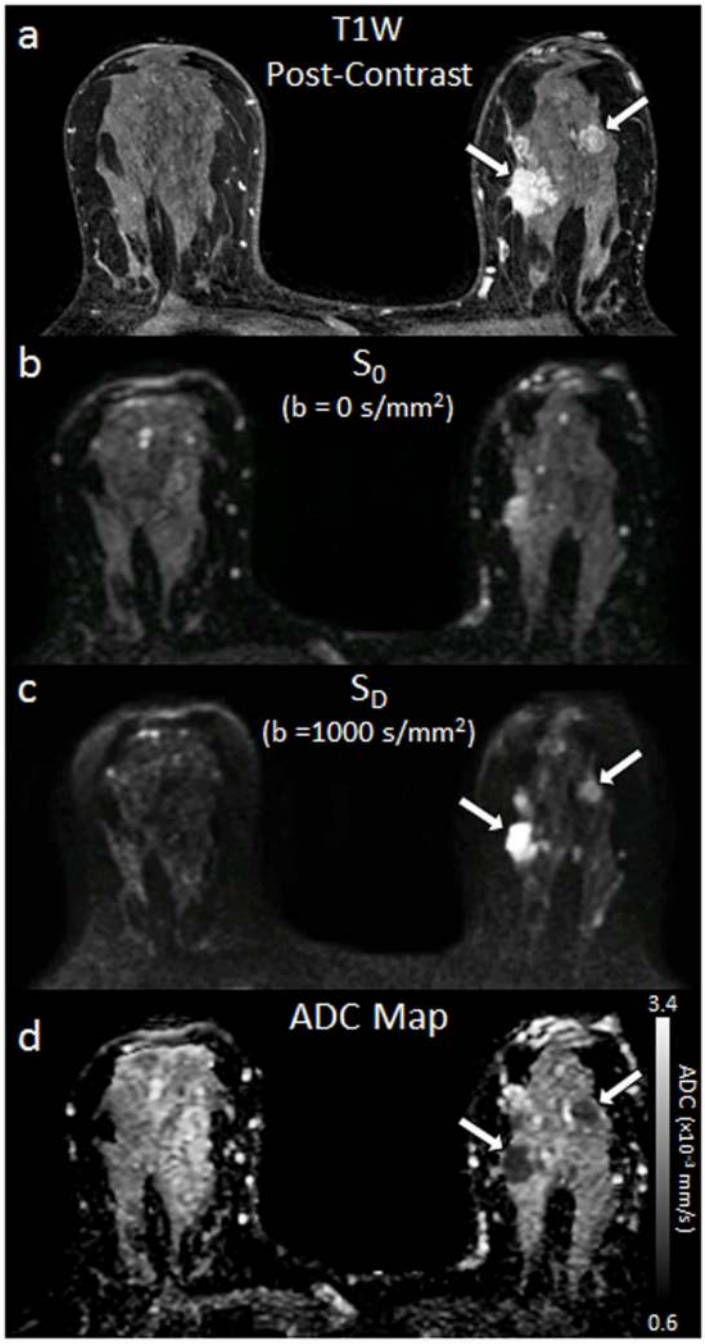

Figure 2.

Example breast images obtained with DWI. Shown are corresponding slices from (a) DCE post-contrast image as reference (b) S_0 with b = 0 s/mm^2 (primarily T2-weighted), (c) S_D with b = 1000 s/mm^2, (d) apparent diffusion coefficient (ADC) map. Invasive tumors (arrows) exhibit reduced diffusivity on DW imaging, appearing hyperintense on S_D image (c) and hypointense on the ADC map (d).

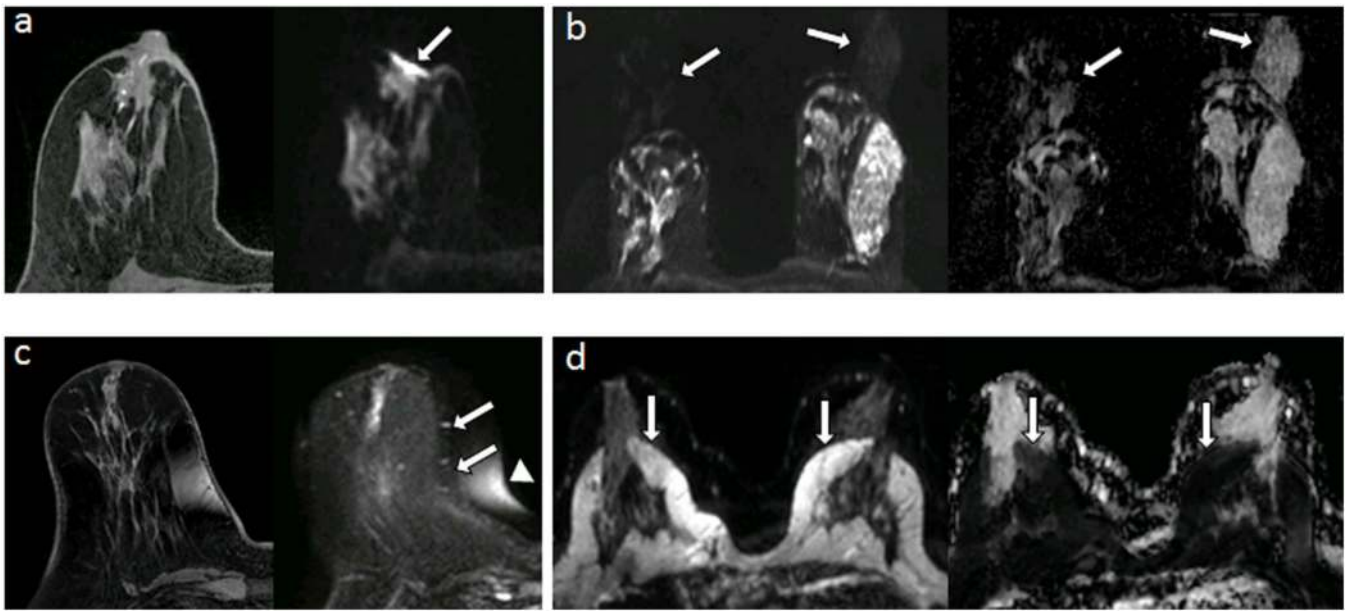

Figure 3.

Common artifacts of breast DWI, illustrated in separate subjects. (a) Magnetic susceptibility artifact (arrow) causing distortion at air/tissue skin surface on DWI (right) compared with undistorted T1-weighted image (left). (b) Nyquist ghost artifact, appearing at N/4 due to parallel imaging undersampling, duplicating signal from the parenchyma on DWI (left) and resulting ADC map (right). (c) Spatial distortion (arrows) and chemical shift artifact (arrowhead) of DWI due to poor shimming compared with undistorted T1-weighted image (left) (d) Detrimental chemical shift artifacts on DWI (left, arrows) due to poor fat suppression, causing artifactual reductions of ADC within the breast parenchyma (right, arrows).

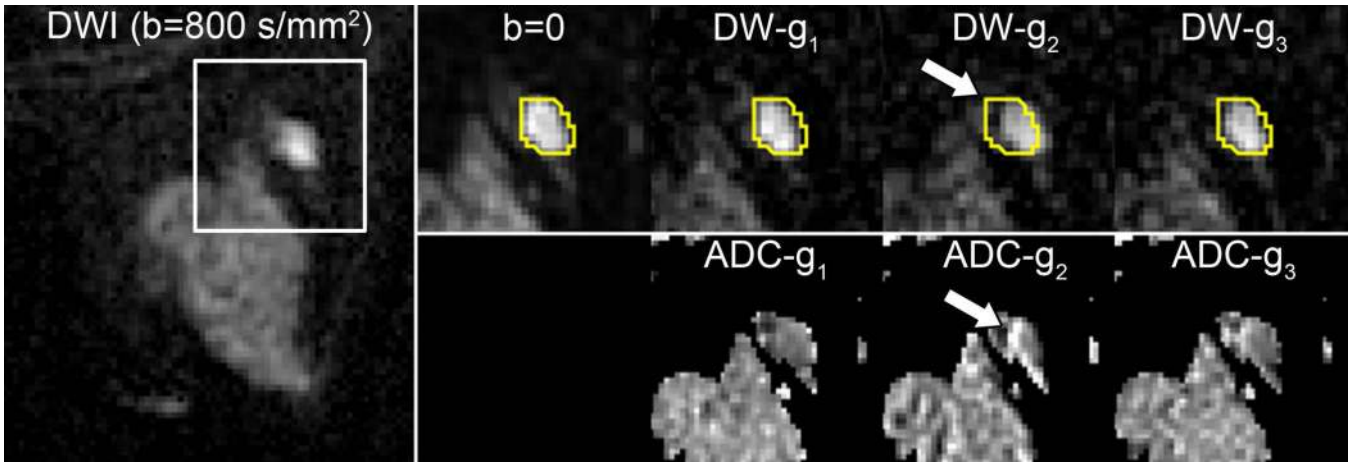

Figure 4.

Spatial misregistration between images within a DWI sequence owing to motion and/or eddy-current artifacts. A breast lesion is visible in the lateral breast on the averaged DW image (b=800 s/mm^2, left). White box shows region of magnification. A contour of the lesion defined on b=0 and propagated to the individual gradient direction DW images for the same slice shows the lesion is shifted (arrow) in the DW-g_2 image (obtained with diffusion gradients applied in the g_2 direction) with respect to the b = 0 s/mm^2 image and other b = 800 s/mm^2 images (obtained with gradients in the orthogonal g_1 and g_3 directions), owing to eddy-current effects. This misalignment causes an artifactual increase in ADC at the edge of the lesion on the corresponding ADC map (below).

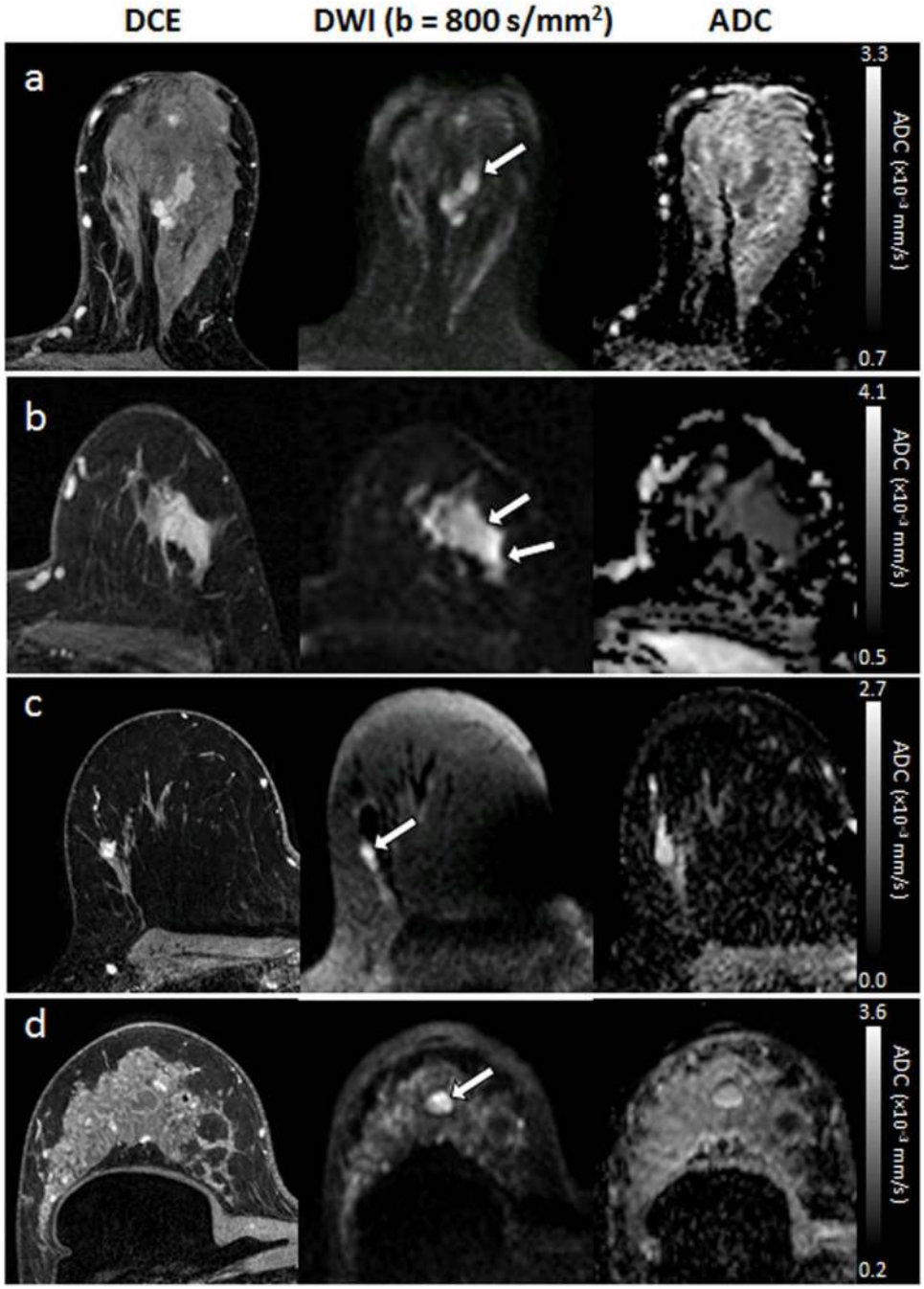

Figure 5.

Examples of different breast lesion pathologies shown on DCE and DWI. Each exhibits hyperintensity on DWI (arrows). (a) 32-mm invasive ductal carcinoma (mean ADC = 1.24 $\times 10^{-3}$ mm^2/s). (b) 34-mm ductal carcinoma in situ (mean ADC = 1.42 $\times 10^{-3}$ mm^2/s). (c) 8-mm fibroadenoma (mean ADC = 1.91 $\times 10^{-3} mm^2/s$). (d) simple cyst (mean ADC = 2.23 $\times 10^{-3}$ mm^2/s).

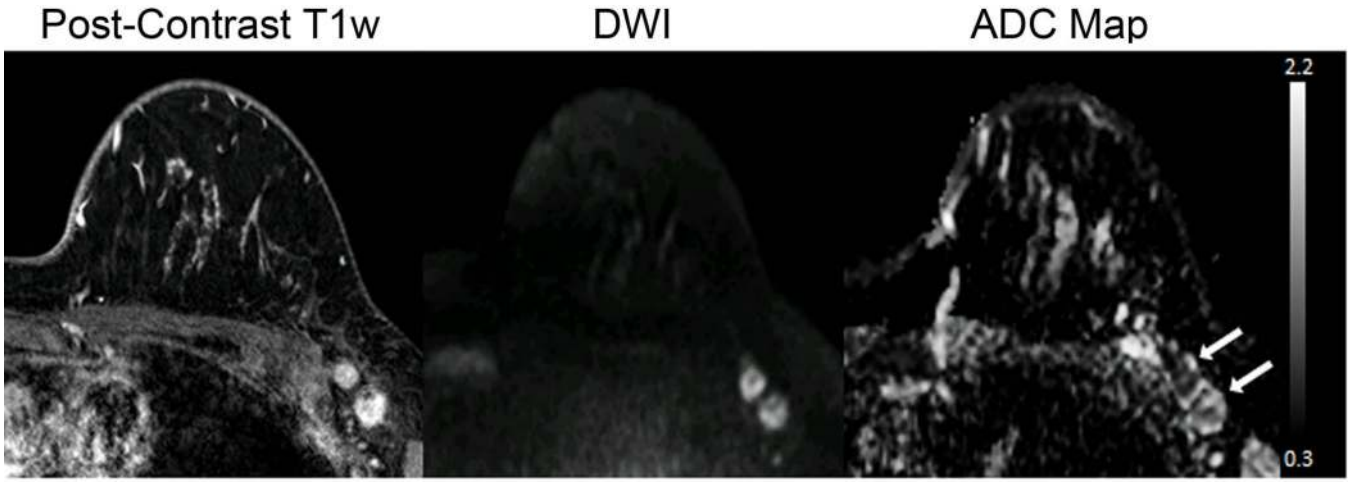

Figure 6.

Axillary metastasis. A 31-year-old woman underwent staging MR imaging after newly diagnosed invasive ductal carcinoma in the left breast. Multiple abnormal level 1 axillary lymph nodes with biopsy proven axillary node metastasis are present in the left axilla, seen as enhancement on the post-contrast T1-weighted image and as hyperintense on the DW (b = 1000 s/mm^2) image due to restricted diffusion. The ADC map demonstrates corresponding low values, with ADC = 0.83 ×10^{-3} mm^2/s and ADC = 1.17 ×10^{-3} mm^2/s for the anterior and posterior nodes, respectively (arrows).

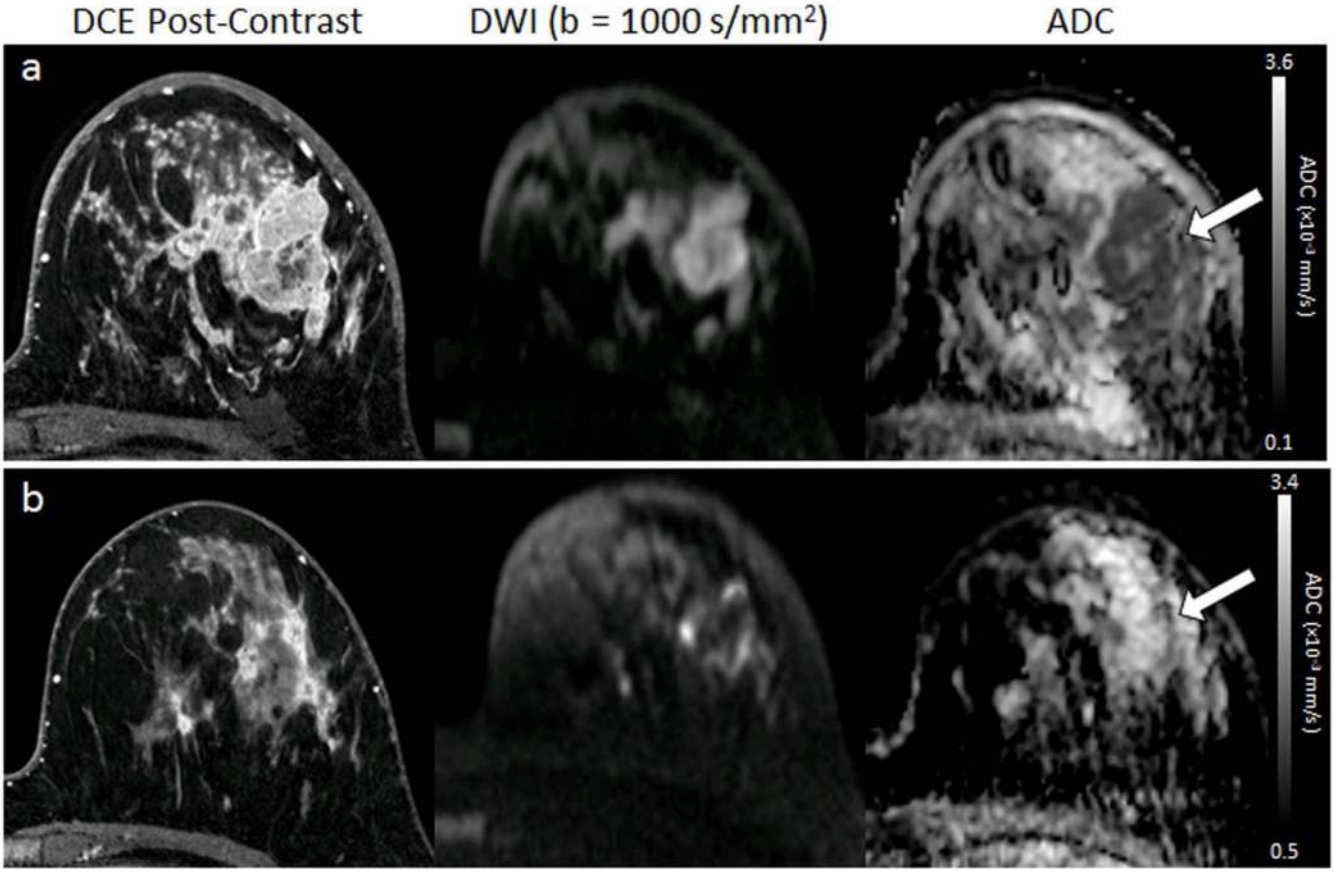

Figure 7.

Serial DWI tumor measures in a 32-year-old woman undergoing chemotherapy for invasive ductal carcinoma. DCE MR images (left) are shown for reference, along with DW (b= 1000 s/mm^2) images (middle) and ADC maps (right) for the corresponding location. (a) Pretreatment, the tumor region exhibits restricted diffusion, with hypointensity on the ADC map (arrow) and mean ADC = 1.01 ×10^{-3} mm^2/s. (b) Mid-treatment after 2 months (4 cycles) of chemotherapy, the tumor region has decreased in size on DCE and increased in ADC (mean ADC = 1.63 ×10^{-3} mm^2/s) suggesting effective treatment. The subject showed a complete pathologic response at the end of neoadjuvant therapy.

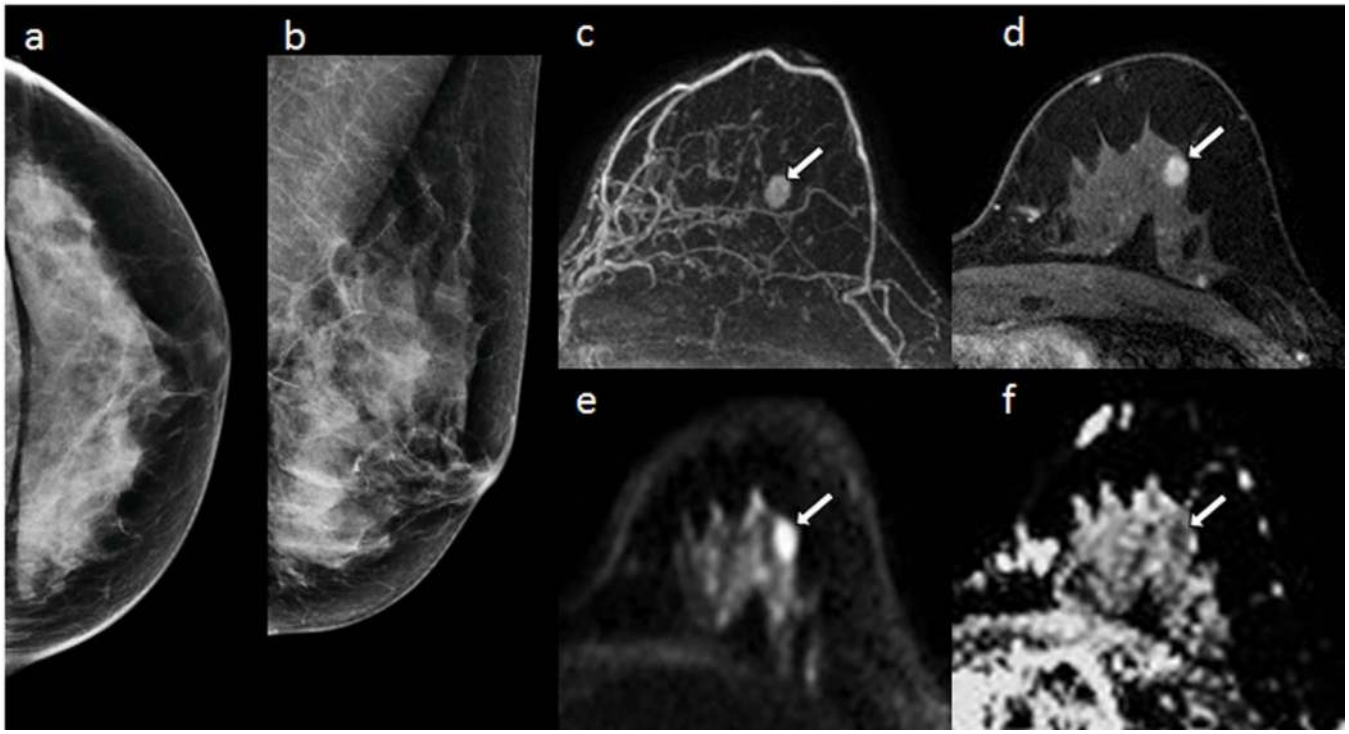

Figure 8.

58-year-old women with dense breasts and mammographically occult invasive ductal carcinoma. Patient underwent high-risk screening MRI because of a strong family history of breast cancer. Shown are (a,b) negative x-ray mammogram (a) cranio-caudal and (b) mediolateral oblique views; DCE (c) maximum intensity projection and (d) T1-weighted dynamic contrast-enhanced MR image, showing an enhancing 8-mm mass (arrow); (e) axial DW image (b value = 800 s/mm^2) showing hyperintensity (arrow), and (f) apparent diffusion coefficient (ADC) map showing low diffusivity of lesion (arrow) (mean ADC = 1.45 ×10^{-3} mm^2/s). (Adapted from McDonald ES, Hammersley JA, Chou SS, et al. Performance of DWI as a Rapid Unenhanced Technique for Detecting Mammographically Occult Breast Cancer in Elevated-Risk Women With Dense Breasts. AJR 2016;207:1–12; with permission.)

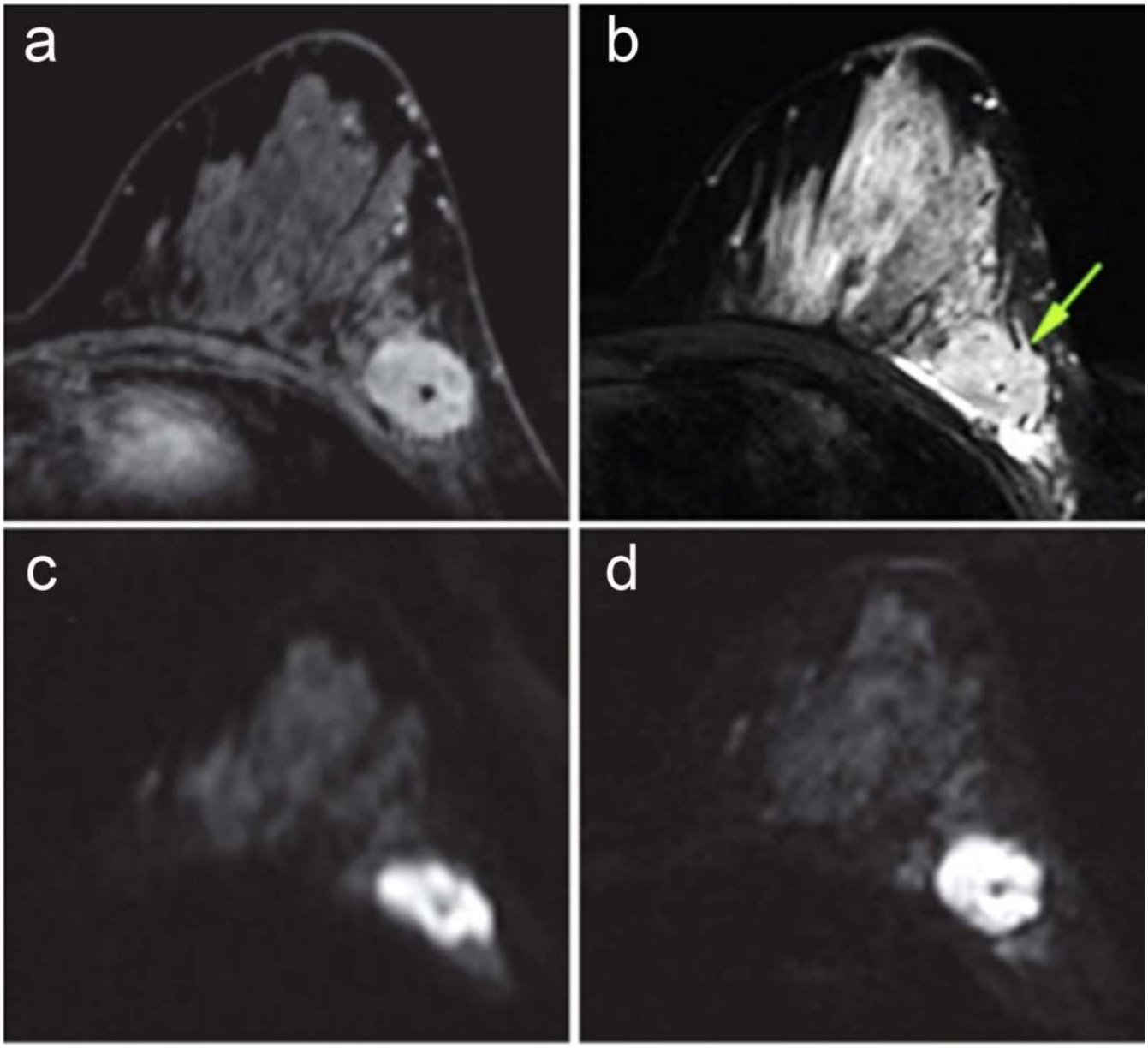

Figure 9.

Comparison of readout-segmented and single-shot EPI breast DWI images in 37-year-old woman with breast cancer (invasive ductal carcinoma, grade 3). (a) Contrast-enhanced T1-weighted MR image, (b) T2-weighted short inversion time inversion recovery image, and DW images with b = 850 sec/mm^2 obtained with (c) single-shot echo-planar imaging, and (d) readout-segmented echo-planar imaging. Significantly stronger geometric distortion artifacts can be seen on (c) single-shot echo-planar image compared with (d) readout-segmented echo-planar image and (b) distortion-free reference STIR image. (d) Readout-segmented echo-planar image also provides significantly higher anatomic detail than (c) single-shot echo-planar image because of reduced T2* blurring. Arrow = malignant lesion. (Adapted from Bogner W, Pinker-Domenig K, Bickel H, et al. Readout-segmented echo-

planar imaging improves the diagnostic performance of diffusion-weighted MR breast examinations at 3.0 T. Radiology. 2012;263(1):64–76; with permission.)

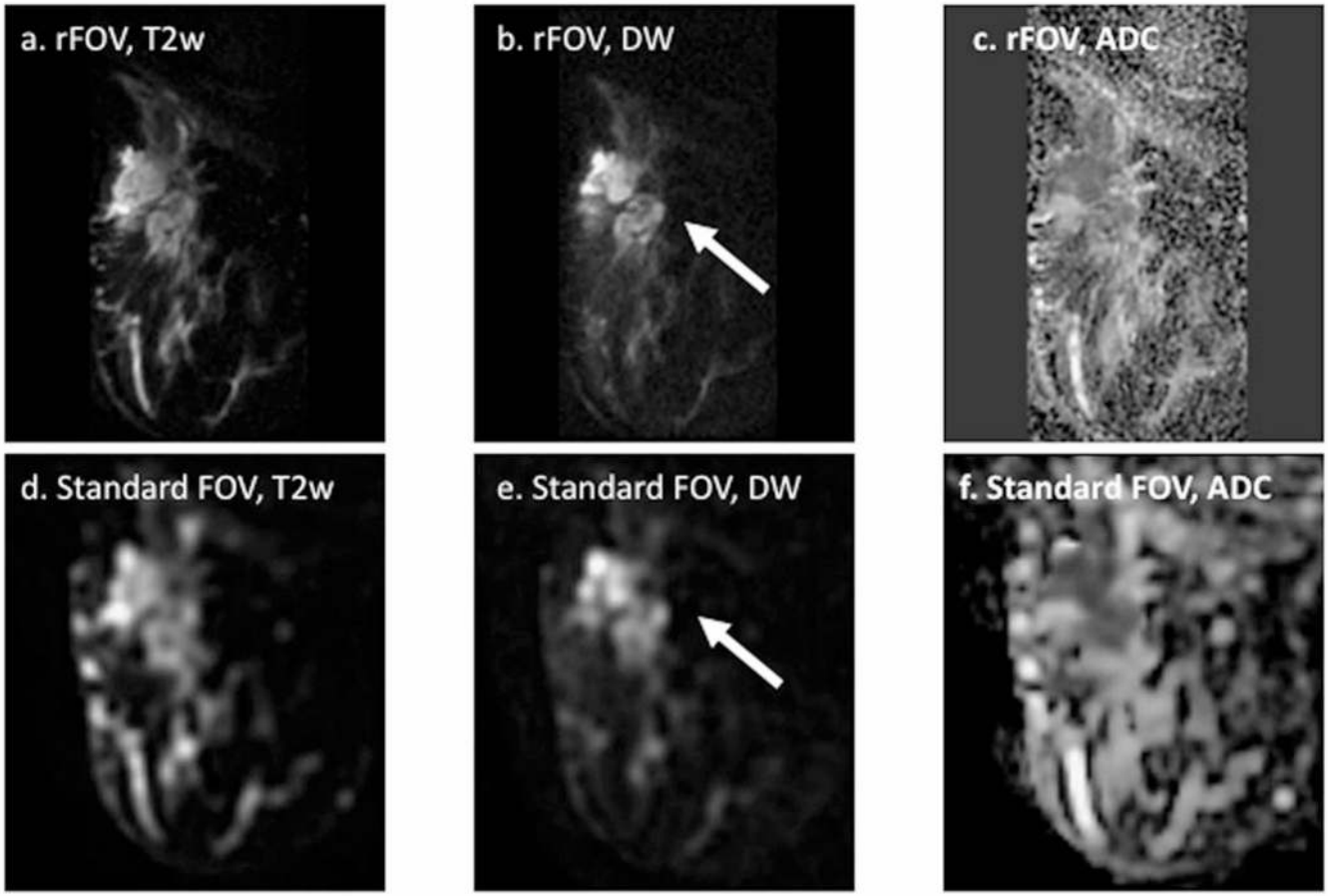

Figure 10.

Reduced field of view (rFOV) diffusion-weighted imaging in a patient with locally advanced breast cancer. Shown are rFOV (a) T2-weighted (T2w) b = 0 image, (b) diffusion-weighted (DW) b=600 s/mm2 image, and (c) ADC map compared to standard-FOV (d) T2w b=0 image, (e) DW b=600 s/mm2 image, and ADC map. The rFOV images provide improved depiction of morphologic detail, intra-tumor heterogeneity, and lesion conspicuity. Arrows = malignant lesion. (Adapted from Singer L, Wilmes L, Saritas E, et al. High-Resolution Diffusion-Weighted Magnetic Resonance Imaging in Patients with Locally Advanced Breast Cancer. Acad Radiol. 2012; 19(5): 526–534; with permission.)

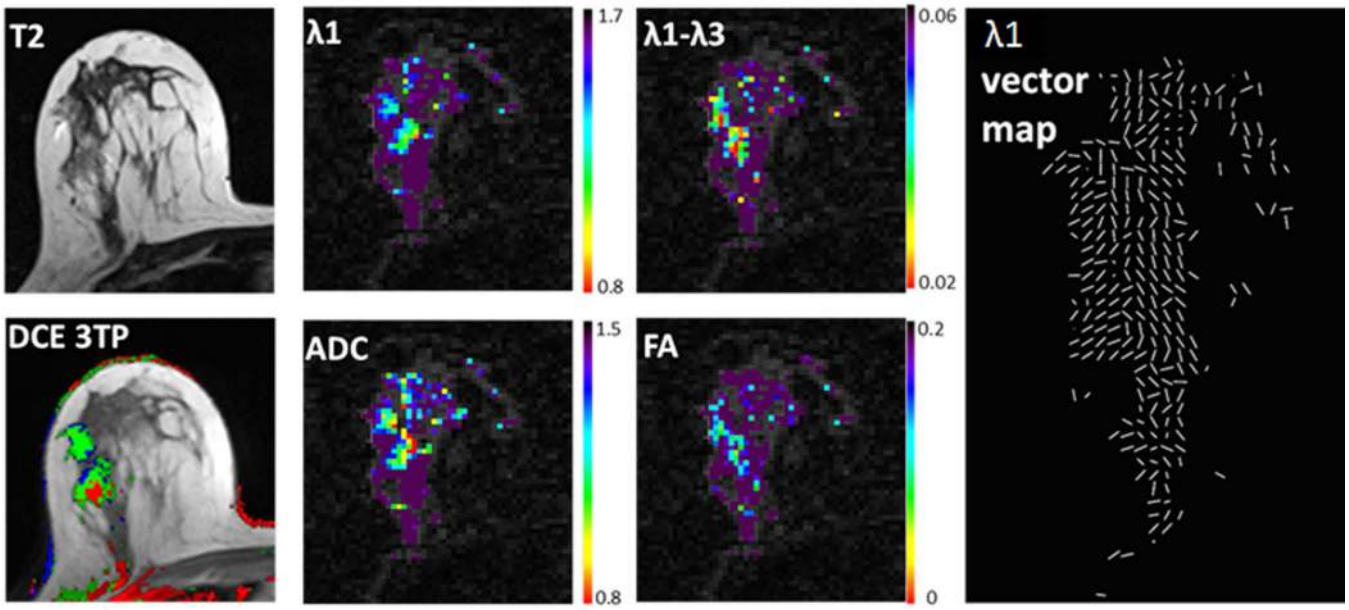

Figure 11.

Example breast DTI analysis. Images and parametric maps of a 57-year-old patient with two lesions of high grade DCIS. T2-weighted, DCE-derived three-time-point (3TP) images and DTI-derived parametric maps of λ_1, ADC, λ_1- λ_3 and FA. λ_1, ADC and λ_1-λ_3 are in units of 10^{-3} (mm^2/s) and presented using a parametric threshold. Corresponding λ_1 vector map depicts direction of maximal diffusivity for each voxel.

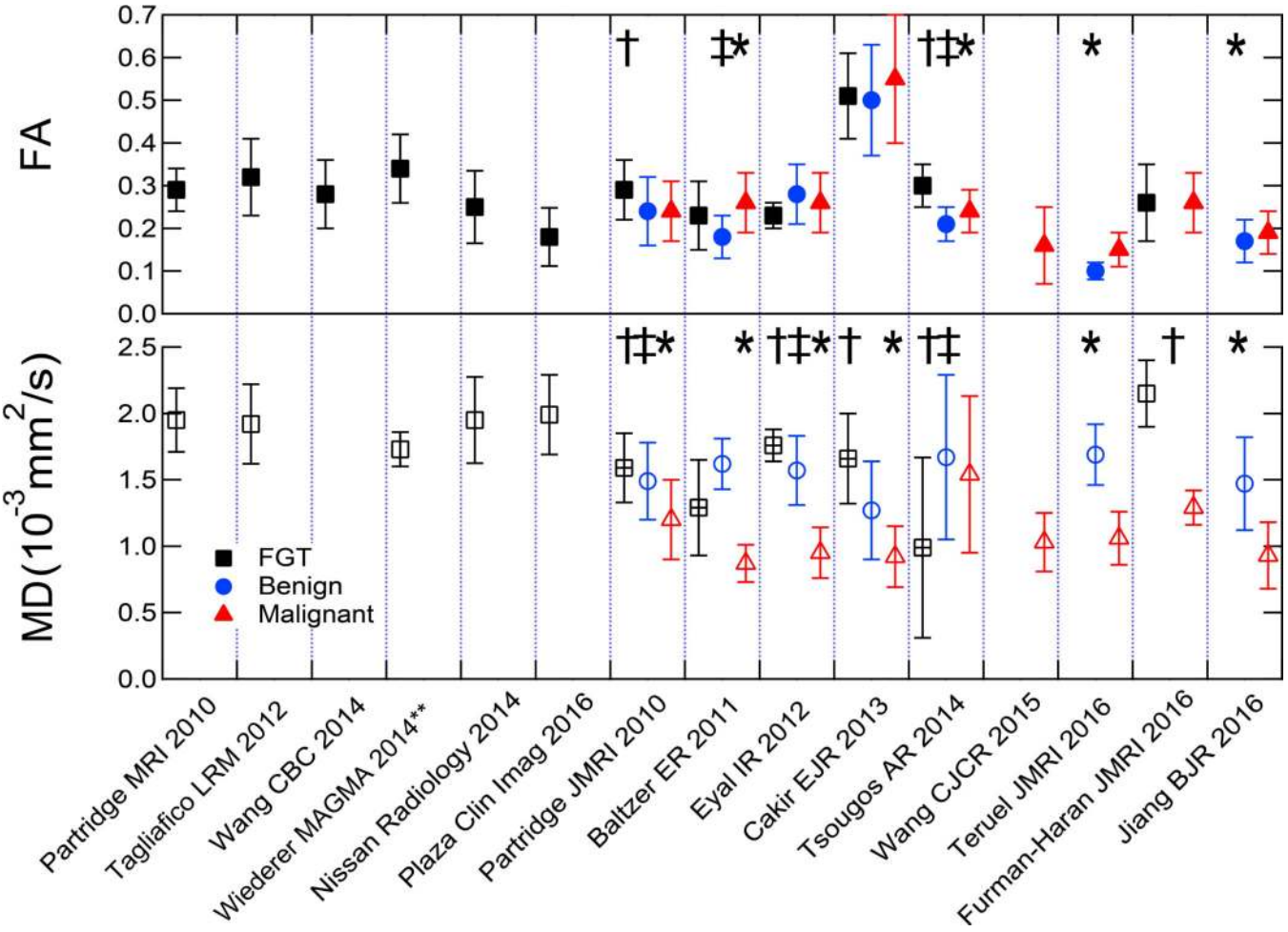

Figure 12.

Summary of lesion measures in multiple breast DTI studies. Plots show mean diffusivity (MD) and fractional anisotropy (FA) values for FGT, benign, and malignant breast tissue across multiple studies. Parameters from showing significant differences between FGT and malignant (†), FGT and benign (‡), and benign and malignant (*) tissue are indicated. MD plot indicates differences between FGT values from patients ('+' square) than those from controls (open square). **Values shown for Wiederer study are weighted averages of reported 'low' and 'high' metrics based on provided values and volume fractions.

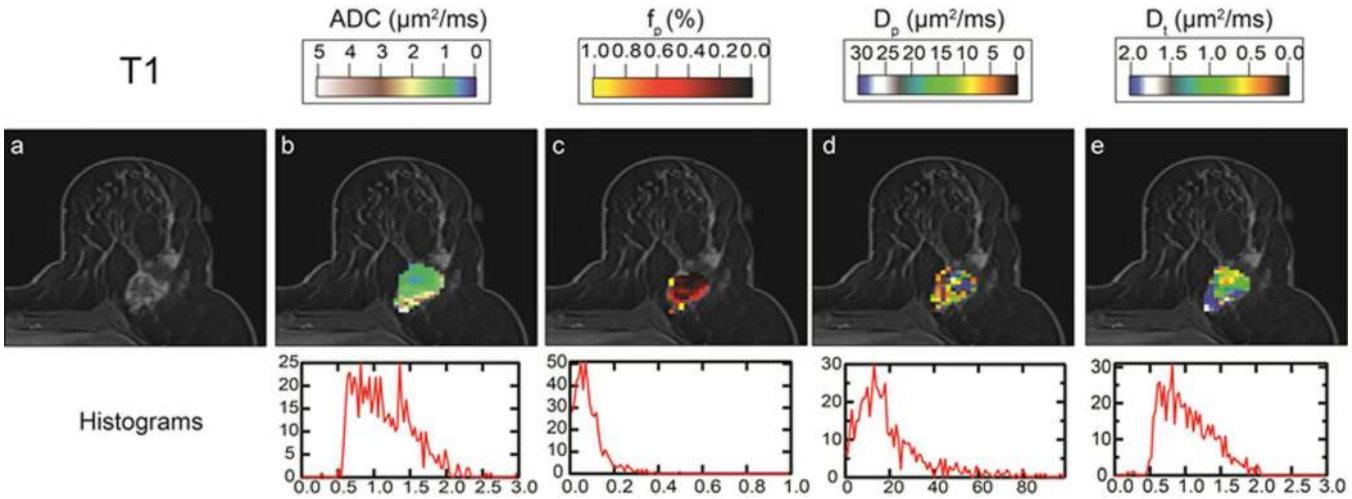

Figure 13.

Intravoxel incoherent motion (IVIM) MRI of an invasive lobular carcinoma (ILC) lesion. (a) Post contrast T1-weighted image, providing background for overlaid (b) apparent diffusion coefficient (ADC), (b) perfusion fraction (f_p), (c) pseudodiffusivity (D_p), and tissue diffusivity (D_t) parametric maps. Full lesion volume histograms for each parameter are shown under the corresponding panels. The lesion shows high central cell density (low ADC, D_t) and high peripheral vascularity (high f_p), in agreement with the appearance in T1 post-contrast imaging (a).

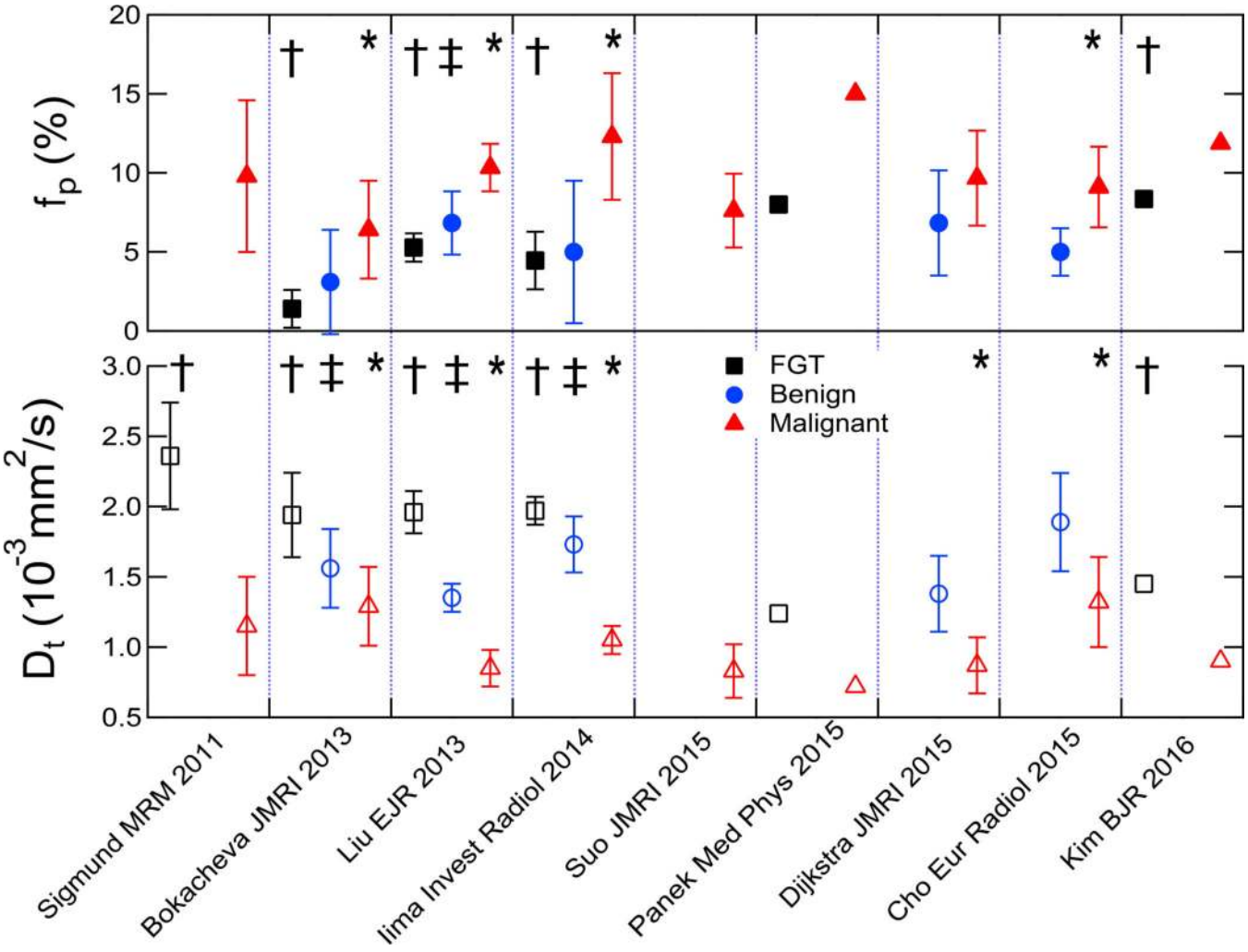

Figure 14.

Summary of lesion measures in multiple breast IVIM studies. Plots show tissue diffusivity (D_t) and perfusion fraction (f_p) values for FGT, benign, and malignant breast tissue across multiple studies. Parameters from showing significant differences between FGT and malignant (†), FGT and benign (‡), and benign and malignant (*) tissue are indicated.

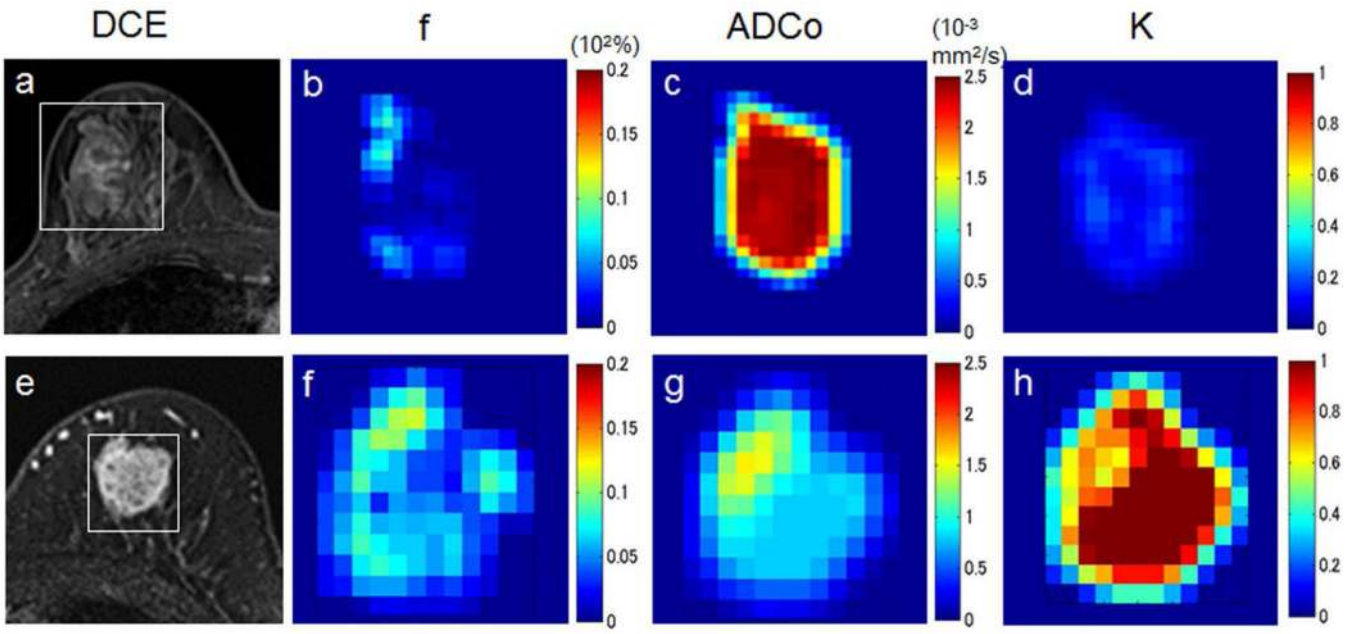

Figure 15.

Example breast IVIM/DKI analysis. Images and parametric maps in two patients with breast lesions. Upper row: Fibroadenoma in a 34-year-old woman. (a) Dynamic contrast-enhanced image shows weak and heterogeneous enhancement in the lesion (white box, area covered by parametric maps). (b) The f map shows very low perfusion in the lesion center, with slightly higher values visible in the left bottom and the upper parts. (c) The ADC_0map shows high and homogeneous values throughout the lesion center, while the K map (d) shows very low values in the center. Such a high ADC_0/low K pattern highly suggests the presence of a free-diffusion tissue component. Lower row: Invasive ductal carcinoma in a 74-year-old woman. (a) Dynamic contrast-enhanced image shows strong and heterogeneous enhancement in the lesion (white box, area covered by parametric maps). (b) High f values are observed in the peripheral area of the tumor. (c) The ADC_0 values are low in the lesion, reflecting high tumor cellularity. In contrast, the K map (d) shows very high values, suggesting some diffusion hindrance effect (possibly from cellular membrane) of the lesion. (Courtesy of Mami Iima, MD, PhD, and Masako Kataoka, MD, PhD, Department of Diagnostic Imaging and Nuclear Medicine, Graduate School of Medicine, Kyoto University, Japan.)

Table 1

Summary of study characteristics for breast DTI publications to date.

Author	Healthy Tissue (n)		Field Strength (T)	b-values (s/mm^2)	Directions (n)	TE (ms)
Partridge, 2010 (108)	12		1.5	0, 600, 1000	6	71.5
Tagliafico, 2012 (109)	60		3.0	0, 1000	32	min
Nissan, 2014 (71)	45 *		3.0	0, 700	30	120
Wang, 2014 (121)	7		1.5	0, 400–1000	6, 15, 31	min
Wiederer, 2014 (110)	7		3.0	0, 500	6	74
Plaza, 2016 (77)	21		3.0	0, 600	6	80–120
	Malignant (n)	Benign (n)				
Partridge, 2010 (112)	76	29	1.5	0, 600	6	71.5
Baltzer, 2011 (114)	54	17	1.5	0, 1000	6	70
Eyal, 2012 (116)	33	20	3.0	0, 700	30–64	120
Cakir, 2013 (115)	30	25	3.0	0, 1000	16	55
Tsougos, 2014 (113)	33	18	3.0	0, 600	6	63.7
Wang, 2015 (119)	64 **	0	1.5	0, 600	6	min
Teruel, 2016 (118)	38	34	3.0	0, 700	30	85
Furman-Haran, 2016 (117)	24	0	3.0	0, 700	30–64	90, 120
Jiang, 2016 (27)	59	29	1.5	0, 1000	6	90

* lactating women

** Wang 2015; 53 invasive, 11 DCIS reported separately (invasive measures only shown on plot Figure 12)

Abbreviation: min=minimum

Table 2

Summary of study characteristics for breast IVIM publications to date.

Author	Malignant (n)	Benign (n)	Healthy Tissue (n)	Field Strength (T)	b-values (s/mm^2)	# b-values	TE (ms)
Sigmund, 2011 (124)	24		20	3.0	0, 30, 70, 100, 150, 200, 300, 400, 500, 800	10	103
Bokacheva, 2013 (125)	26	14		3.0	0, 30, 60, 90, 120, 400, (450 in 7 cases), 600, 800, 1000	9	56.4
Liu, 2013 (126)	40	71 *	39	1.5	0, 10, 20, 30, 50, 70, 100, 150, 200, 400, 600, 1000	12	66
Iima, 2014 (132)	15	8		3.0	3, 5, 10, 20, 30, 50, 70, 100, 200, 400, 600, 800, 1000, 1500, 2000, 2500	16	77
Suo, 2015 (128)	30			3.0	0, 50, 100, 150, 200, 500, 800	7	67
Panek, 2015 (130)	21		5	3.0	0, 50, 100, 200, 300, 400, 600, 800, 1000, 1150	10	79
Dijkstra, 2015 (129)	165	41		1.5	0, 50, 200, 500, 800, 1000	5	91
Cho, 2015 (96)	50	12		3.0	0, 30, 70, 100, 150, 200, 300, 400, 500, 800	10	103
Kim, 2016 (131)	275			3.0	0,30, 70, 100, 150, 200, 300, 400, 500, 800	10	43

* includes 30 cysts